



SINTEF

Project Report

An Engineering Equation for Thermal Ice Loads on Dams

Author(s)

Christian Petrich

Irina Sæther

Report Number

2025:00427 — Unrestricted

Client(s)

Fornybar Norge

Norges vassdrags- og energidirektorat



SINTEF Narvik
 Address:
 Rombaksveien 47
 8517 Narvik
 Telephone: +47 40005100
 info@sintef.no
 Enterprise Number:
 962951511

Project Report

An Engineering Equation for Thermal Ice Loads on Dams

KEYWORDS:
 Hydropower
 Design Load
 Ice Load
 Modeling

VERSION
 2.0

DATE
 10th April 2025

AUTHOR(S)
 Christian Petrich
 Irina Sæther

CLIENT(S)
 Fornybar Norge
 Norges vassdrags- og energidirektorat

CLIENT'S REFERENCE

PROJECT NUMBER
 402000011

NUMBER OF PAGES AND ATTACHMENTS
 41

ABSTRACT

This research project was jointly financed through the project Dam Safety in a Holistic Perspective (DHSP) and the Norwegian Water Resources and Energy Directorate (NVE). The goal was to derive an engineering-friendly assessment of thermal ice loads on dams based on an energy-conserving ice growth model and published relationships between ice temperature changes and compressive stress. This report presents both a probabilistic and a deterministic approach to the problem and presents associated design solution. Key results include a physically-based justification for the shape of the ice load equation, and the presentation of an ice load probability distribution that accounts for ice-free years. It is suggested that further improvements to ice load predictions consider regional differences of the snow cover. Also, the data basis of measured thermal ice loads should be improved in Norway.

PREPARED BY
 Christian Petrich

SIGNATURE

CHECKED BY
 Bård Arntsen
 Megan O'Sadnick

SIGNATURE

APPROVED BY
 Roy Antonsen

SIGNATURE

REPORT NUMBER
 2025:00427

ISBN
 978-82-14-07487-1

CLASSIFICATION
 Unrestricted

CLASSIFICATION THIS PAGE
 Unrestricted

Document History

VERSION	DATE	VERSION DESCRIPTION
1.0	2023-05-31	Original Draft
2.0	2025-04-10	Revised Version

Contents

Preface	5
1 Overview	6
1.1 Motivation	6
1.2 Background	7
1.2.1 Modeling	7
1.2.2 Annual Peak Ice Load Probability Distribution	8
1.3 Content of Report	10
1.3.1 Probabilistic Model	10
1.3.2 Deterministic Model	10
1.3.3 Explicit Equation	11
1.3.4 Snow	11
2 Materials and Methods	12
2.1 Temperature	12
2.2 Calculation of the Freezing Index	13
2.3 Rheological Model of Thermal Ice Loads	14
2.4 Model of Ice Growth and Ice Temperature	14
2.4.1 Model Implementation	15
2.5 Peak Ice Load Probability Distribution	17
2.6 Probabilistic Model	18
2.7 Air Temperature Characteristics	18
2.8 Deterministic Model	19
2.9 Explicit Equation	20
3 Results	22
3.1 Freezing Index versus Freezing Degree Days	22
3.2 Genesis of a Thermal Ice Load Event	23
3.3 Probabilistic Model	24
3.3.1 Snow Depth Parameterization	24
3.3.2 Probabilistic Model Process	25
3.3.3 Line Load Peak Distribution Function	26
3.3.4 Design Line Load	26
3.3.5 Ice Stress at Peak Load	29
3.4 Deterministic Model	29
3.4.1 Model Input	29
3.4.2 Design Line Load	32
3.5 Explicit Equation	32
3.5.1 Design Line Load	32

4 Discussion **35**

4.1 Explicit Equation 35

4.2 Peak Ice Load Probability Distribution 35

4.3 Other Effects 36

5 Conclusion **37**



Preface

This research project was jointly financed through the project Dam Safety in a Holistic Perspective (DHSP) and the Norwegian Water Resources and Energy Directorate (NVE). It both gained and suffered from the constructive input of a very engaged industry reference group. The original intention of this project was to address the regional differences of thermal ice loads across Norway with focus on coastal reservoirs as one might assume that those should have systematically lower peak loads than implied by the design guidelines. However, the focus shifted about half-way through the project as the desire within the reference group was to investigate the whole spectrum of ice loads throughout Norway. Toward the end of the project period the desire was voiced to validate the assumptions underlying this project. Hence the final product is a compromise, as usual for a research project. Some aspects have been brought to completion, while others have only been touched upon. This report focusses on the completed work that is most directly applicable to thermal ice loads. Of particular interest might be the comparison between a deterministic approach and a probabilistic approach which incidentally led to nearly identical results. The deterministic approach was further reduced into a compelling simple explicit equation. Aspects related to ice load probability distribution may also be of wider significance since, unlike possibly other parts of the world, a fair share of reservoirs in Norway experience ice loads not in every winter. In future work, the most value might possibly be gained by investigating snow conditions across the country. While a large database of publicly contributed snow-on-ice observations exists, preliminary work done in this study suggests that ice observers have generally not focused on the characterization of snow on ice. Hence, each snow-related aspect of an observation has been quality controlled. It turned out that a promising way of doing this is with a plausibility check against a buoyancy-considering snow-on-ice model, i.e., work that started late and was not possible to complete in this project. An unmet open need is to develop a better data set of field measurements of thermal ice loads throughout Norway.

Chapter 1

Overview

1.1 Motivation

Static ice loads on dams occur when a dam constrains the movement of an ice cover. The causes thought to be most relevant for static ice loads are water level changes and air temperature changes (Carter et al., 1998). This report presents results from a modeling effort of ice loads on vertical concrete dam faces in response to constrained thermal expansion of an ice cover. Ice loads are known to damage dams. However, there are no reported dam failures due to static ice loads in recent decades even though field investigations and theoretical investigations suggest that ice loads may exceed those specified in regulations. From a Canadian perspective, Morse et al. (2009) summarized the situation as follows:

Whereas recent studies (Carter et al., 1998; Comfort et al., 2003) indicate that ice forces could be well above those recommended by the Canadian Dam Association (150 kN/m), some public agencies have, in some cases, actually reduced their design values for smaller dams to 100 kN/m. If these dams are truly unsafe, mitigation measures should be defined and applied as soon as possible. On the other hand, should ice forces not present a safety risk (as is suggested by the fact that no known dam has failed in this manner), then investing in dam reinforcement may be a misuse of public funds. Thus, it is important to know what constitutes a safe, realistic and practical design value for ice thrust against linear structures.

The current Norwegian regulations (NVE, 2003) stipulate that a thermal ice load of 100 to 150 kN/m be used across Norway, depending on local ice conditions, without quantitative guidance on how to set the limit. Dams in the lowest breach consequence class (bruddkonsekvensklasse) can use 100 kN/m irrespective of ice conditions. Values below 100 kN/m may be used based on a case-by-case assessment. Ice loads can exceed thermal ice loads in reservoirs with significant water level fluctuations (defined as daily fluctuations $\geq \pm 0.2$ m, presumably based on Lia et al. (2002)). In this case the NVE guidelines stipulate an upper limit on the combined ice forces. The given equation apparently stems from the theoretical reasoning of Carter et al. (1998) who define an upper limit on ice forces in a deformed ice cover containing unfrozen cracks: an ice cover can be assumed to have cracks parallel to the dam at predictable intervals that depend on ice thickness. The maximum load transferred by the ice perpendicular to the dam is the force required to displace the ice blocks between the cracks against buoyancy. I.e. the ice cover will start to form rubble at higher loads rather than push into the dam. The limiting line load LL is given as a function of ice thickness H as

$$LL = 250 H^{1.5}, \quad (1.1)$$

where H is in m and LL in kN/m. NVE (2003) further states that the ice thickness can be calculated from the freezing degree day (FDD) equation

$$H = 0.02 FDD^{0.5}, \quad (1.2)$$



where FDD in $^{\circ}C$ days are the regionally tabulated F_{100} freezing degree days, and H is the ice thickness in m. While the origin of Equation 1.2 is not given, this equation predicted observed ice thickness in reservoirs investigated by Carter et al. (1998) in eastern Canada well. Carter et al. (1998) attribute this equation to Drouin (1976). A co-worker of Drouin in the 1970s, Michel (1971) gave several ice growth equations, among them Equation 1.2, which was labeled “average lake with snow”. However, the same equation has also been used in completely different context of ice growth, e.g. in the Caspian Sea (Palmer & Croasdale, 2012). The origin of the 0.2 m threshold for the limit equation of ice loads due to water level fluctuations that is found in the summary of Lia et al. (2002) is unclear. The limiting equation of Carter et al. (1998) (i.e., Equation 1.1) is applicable irrespective of water level fluctuations but requires that the ice cover is deformed (i.e., not a horizontal, flat surface). Previous NVE regulations stipulated ice loads of 100 kN/m, and a study had been conducted to investigate whether this value could be made more correct (Lia et al., 2002). The study concluded that thermal ice loads up to 135 kN/m had been measured in a reservoir near Narvik, and that there are no reports in the investigated literature of measured thermal ice loads in excess of 150 kN/m. In addition, the report concludes that higher loads have been observed as a result of water level fluctuations and suggests the use of the line load limit equation of Carter et al. (1998) (Equation 1.1). Since the publication of the regulations, Comfort et al. (2003) pointed out that water level fluctuations exceeding ice thickness seem to reduce maximum ice loads. Sæther (2019) remarked that several seasons of additional ice load measurements in Narvik had resulted in line loads below 150 kN/m. Petrich and Arntsen (2018) modeled thermal ice loads at 1700 locations across Norway assuming the absence of a snow cover and found significant regional differences. While some regions experienced peak loads well below 100 kN/m, others had average peak thermal loads exceeding 200 kN/m. Thermal ice loads depend on both ice thickness and temperature fluctuations, both of which have regional dependencies. Implicitly underlying the current regulatory regime in Norway (NVE, 2003) is the premise that ice in Norwegian reservoirs can be assumed to be typically snow-covered. The original goal of this study was to model thermal ice loads for temperature conditions across Norway, assuming a snow cover comparable to Equation 1.2 in combination with an ice load model similar to Petrich and Arntsen (2018).

1.2 Background

1.2.1 Modeling

Measurements of ice loads exist, were documented at different level of detail and have been reviewed elsewhere (e.g. Adolphi & Eriksson, 2013; Lia et al., 2002; Sæther, 2019). Among the more recent measurements are measurements in China (Qiu et al., 2024), Sweden (Hellgren et al., 2022), Norway (Foss, 2017; Petrich et al., 2020) and Canada (Comfort et al., 2003; Taras et al., 2011). While Gebre et al. (2013) concluded that there was still no consensus on how to model thermal ice loads, the numerical treatment outside of empirical parameterizations seems to have concentrated on elasto-viscous models since.

Thermal stress in a confined, solid ice specimen is governed by a balance of thermal expansion, and the elastic and creep properties of ice. Sinha (1983) described such a rheological model for small samples of ice. This model had subsequently been shown to reproduce thermal stresses measured in a hydropower reservoir, although underestimating their magnitude (Côté et al., 2016). The model of Sinha (1983) contains a numerically inconvenient delayed elastic stress term, and Kharik et al. (2018) found in a dedicated study that a numerically simpler elasto-viscous model would be sufficient for stress modeling in reservoirs. Elasto-viscous models had previously been used to describe ice loads on structures, and their proposed forms differed mainly in the treatment of the temperature-dependence of creep (e.g. Azarnejad & Hruday, 1998; Bergdahl, 1978; Cox, 1984; Fransson, 1988; Petrich et al., 2015). The present study follows the approach of Cox (1984), which was developed for a wide range of temperatures, had been calibrated to observations in Norway (Petrich et al., 2015), and has been shown to be able to reproduce measured thermal ice loads in two winter seasons (Petrich et al., 2020). Even where ice load measurements were performed at concrete dams that present a relatively simple boundary, it had been established that spatial stress inhomogeneity exists along a dam (e.g. Morse



et al., 2009) and that the highest stresses are not measured simultaneously along the whole dam. This gives rise to a distinction between local and global ice load (e.g. Côté et al., 2016; Morse et al., 2011; Petrich et al., 2015, 2020; Taras et al., 2011). This report considers local thermal ice loads that are relevant to the stability of individual sections of a dam.

There are approaches toward ice modeling that differ systematically from the approach taken in this study. As an example to highlight that suitable approaches may differ across the globe due to climatic conditions, we take a model developed by Xie and apparently successfully used in China (Qiu et al., 2024; Xie, 1992): that model is an empirical equation that describes thermal ice pressure on structures such as dams in terms of air temperature increase from 8 to 14 o'clock, morning air temperature, snow cover, ice thickness, and reservoir confinement. Since air temperatures in northern Norway are not diurnal in winter there is little doubt that such an approach to thermal ice loads will be of limited utility in this study. However, other empirical approaches could be more applicable (e.g. Comfort et al., 2003).

1.2.2 Annual Peak Ice Load Probability Distribution

One of the tasks of this project is to establish a probability distribution for annual maximum peak thermal line loads, and to use this to determine the expected thermal load with a recurrence rate of 50 years. For this, both an appropriate probability distribution has to be established and proper coefficients need to be found.

In graphical analysis of extreme value distributions, the usual process is to plot the data on probability paper, starting with a test for the normal distribution. If the data look positively skewed or have a long tail, probability paper for the log-normal distribution is tried next. If they are either even more skewed or less skewed, Gumbel or Weibull probability paper would be tried (Santner, 1973).

There is limited precedence for the choice of the distribution function of thermal ice loads on dams. It appears to be customary in Norway to use a truncated log-normal ice load probability density function (Mydland & Eklund, 2021; Sandaker, 2018), based on the description of a model from Sweden (Wilde & Johansson, 2016). Hovde et al. (2018) used a piecewise linear approximation of a truncated log-normal. For the choice of log-normal distribution they refer to the MSc Thesis of Adolfi and Eriksson (2013) who stated that they had chosen a log-normal distribution fitted to available published measurements because the log-normal distribution does not predict negative ice loads and the probability of occurrence decreases with increasing line load magnitude.

Other choices made for probability distributions in a context somewhat related to the present task include the Gumbel distribution to determine the 10 and 100-year Freezing Index across Norway (ISO13793, 2001; Kvande et al., 2023), and the Gumbel and, more recently, Generalized Extreme Value distribution (GEV) for snow loads (Tajet & Grinde, 2022).

The Generalized Extreme Value distribution (GEV) is a particularly interesting distribution to consider if the recurrence of peak values is to be determined. It is known that a large sample of the maxima of boxed data of peak events will converge to the GEV distribution (Jenkinson, 1955). E.g., taking a winter season as a “box” and assuming that there are many load events during a winter season, the distribution of the seasonal maximum load will follow the GEV distribution. Three different types of GEV distributions are distinguished depending on the shape parameter ξ (Fisher & Tippett, 1928). The Fréchet distribution (Type II, $\xi > 0$) has a lower bound, the Reverse Weibul distribution (Type III, $\xi < 0$) has an upper bound, and the Gumbel distribution (Type I, $\xi = 0$) is unbounded. The applicable type depends on the parent distribution that created the peaks within the box (Gumbel, 1954). The domain of attraction for the Fréchet distribution are parent distributions that do not have all of their moments finite, i.e. long-tailed distributions such as Pareto and Cauchy, the domain of attraction for the Reverse Weibul distribution are distributions with a finite upper endpoint, and the domain of attraction for the Gumbel distribution are all the remaining distributions, e.g. normal and log-normal (Papalexiou & Koutsoyiannis, 2013). Unfortunately, it takes many peaks to obtain convergence toward the GEV distribution, making fitting for ξ subject to considerable error (e.g. Papalexiou & Koutsoyiannis, 2013). Also, if the number of peaks in a box is insufficient, the distribution will have more of the character of the parent distribution than that of the GEV distribution (Gumbel, 1954).

Once a distribution is chosen, the parameters need to be estimated from the observed data. The commonly used methods share two main characteristics, i.e. they converge to the true parameters of the distribution in the limit of infinitely large datasets, and none is guaranteed to be “better” than the other for small datasets. A wide range of methods exist, and development of methods is ongoing (e.g. Makkonen & Tikanmäki, 2019). Common methods include a linear fit on a quantile plot, e.g. on probability paper (Probability Plot Method) (Gumbel, 1958), determining the moments of the sample and calculating the parameters from this directly (Method of Moments, MoM) (Pearson, 1936), determining the L-moments rather than conventional moments to calculate the parameters (Probability-Weighted Moments, PWM) (Hosking, 1990; Hosking et al., 1985), and numerically maximizing the log-likelihood function to adjust the parameters to their most probable value given the observed data (Maximum Likelihood Estimator, MLE) (e.g. Coles, 2001).

In any event, data should be plotted in order to assess the quality of a fit because summary statistics may fail to pick up significant characteristics. Anscombe’s quartet is a famous example of a linear fit to four notably different datasets possessing identical statistics (Anscombe, 1973). A time-proven method to evaluate data with respect to a probability distribution is the quantile plot (also called quantile–quantile plot or Q–Q plot), which contains the points

$$\left(\Phi^{-1} \left(\frac{i}{n+1} \right); x_{(i)} \right) \quad \text{for } i = 1, \dots, n, \tag{1.3}$$

where Φ^{-1} is the inverse of the cumulative distribution function (CDF), and the fraction $i/(n+1)$ is commonly referred to as the plotting position of ordered sample $x_{(i)}$ of independent observations (a.k.a. order ranked observations)

$$x_{(1)} \leq x_{(2)} \leq \dots \leq x_{(n)} \tag{1.4}$$

(Coles, 2001). If Φ is the CDF of the reduced variate (e.g., for the normal distribution the reduced variate would be $z_i = (x_i - \mu)/\sigma$) then the quantile plot is identical to a plot on probability paper, and location (μ) and shape parameters (σ) can be derived from intercept and slope of a linear fit to the points (e.g. Gumbel, 1954; Santner, 1973). Makkonen (2006, 2008) argued that the plotting position $i/(n+1)$ is in fact the only correct choice for the purpose of estimating return periods from the data. Estimation of recurrence rates based on plots on probability paper have been discussed by Gumbel (1954) and are widely recognized (e.g. ISO13793, 2001). Interestingly, Gumbel (1954) used s_x to describe the population standard deviation (i.e., division by N) in his derivation of the tabulated coefficients. The derivation in his 1958 (and 2004) work is almost a verbatim copy of that derivation except that s_x is defined as the sample standard deviation (i.e., division by $N - 1$) (e.g. Gumbel, 1958). The stated result expressed in terms of s_x is identical to the 1954 work. Apparently, the presentation of the 1958 work has found entry into the wider literature (e.g. ISO13793, 2001) while the 1954 version is mathematically correct.

There is a fundamental problem of how to deal with winters of no ice, i.e. zero thermal ice loads. Adolfi and Eriksson (2013) used the log-normal distribution to fit the ice load data specifically because, as they state, it is only defined for positive values. While this is an intuitive solution for regions that consistently see ice formation, this approach fails where occasional zero-loads appear because some winters were too warm for ice to form. In this case, a finite number of zero values appears in the observed distribution, rendering the log-normal distribution unsuitable.

Observations that are present but do not provide well-quantified data points can be dealt with in the context of nondetects, i.e. values smaller than a detection limit, through the Probability Plot Method or Regression on Order Statistics (ROS) (Helsel, 2010; Shumway et al., 2002). Unlike the Method of Moments, Probability-Weighted Moments, or Maximum Likelihood Estimator, there is a reasonably straight-forward way of dealing with zero-valued data with Order-Ranked Observations (ORO): using ORO, a distribution is chosen (e.g. Normal, Log-normal, or Gumbel), the CDF of the observations is scaled to be linear, and the parameters of the distribution are determined from slope and intercept derived from least-squares fitting. While records of zeros affect the position of the other observations in the CDF (Equation 1.3), they do not provide data points for the least-squares fit. I.e., the only information retained from them is the number of observations smaller than the smallest non-zero value.

1.3 Content of Report

In this report, the design thermal ice loads for a given location is determined with three different approaches. The design thermal ice load is the annual peak thermal ice loads with a recurrence rate of 50 years, and the location is characterized exclusively by its Freezing Index with 10-year recurrence rate (FI_{10}), of which 1 km gridded data are readily available for Norway. The approaches are:

- fitting design ice load data derived from a probabilistic model to the local freezing index,
- fitting design ice load data derived from a deterministic model to the local freezing index, and
- calculating design ice load data directly from the local freezing index based on an explicit expression derived from the deterministic model.

Only the probabilistic model is able to derive a relationship for any chosen recurrence rate. The relationship between input and output is more obvious in the deterministic model, but it is not clear from the outset whether the result corresponds to a meaningful probabilistic recurrence rate (however, the model described below happens to reproduce the 50-year recurrence rate). The physically-based explicit equation gives a direct result and thereby suggests a functional shape for curve fitting including a physical interpretation of the fitted parameters. However, it is based on significant simplifications that may not apply under all conceivable circumstances. Only the probabilistic model was originally planned for in this project, while the deterministic model and the explicit equation were added in response to requests from the reference group. From an engineering point of view, a simple, physically-based and correct result would be most desirable.

1.3.1 Probabilistic Model

In the the probabilistic model the probability distribution for thermal line loads is calculated for many locations across Norway and fitted to a suitable probability distribution function. The design load at the desired recurrence rate can then be directly calculated from the distribution function. In this model, the daily air temperatures drive a column-model of a lake. As the air temperature cools the water, ice starts to form. Air temperature variations propagate through the ice and modulate the ice growth rate. (Standard numerical methods are used to perform this calculation.) The ice temperature changes at different depths inside the ice are converted to ice stresses with a rheological model (which is taken from the literature), and the stresses are integrated through the thickness of the ice to determine the daily development of the line load. From each winter only the peak line load is retained. A probability distribution function is fitted to the load simulations of 31 winters, and the line load with 50-year recurrence rate is determined from this. Together with the 10-year Freezing Index of this location, this design line load provides one data point in a scatter plot. The scatter plot is filled with calculations of approximately 2000 reservoir locations across Norway, and an empirical curve is fitted to the plot. This curve describes the relationship between 50-year design line load and local 10-year Freezing Index.

1.3.2 Deterministic Model

Key parameters determining thermal ice loads are ice thickness, ice temperature, and ice temperature rise. First, statistical relationships are sought relating these three parameters to the 10-year Freezing Index of the desired location. For this, daily air temperature data are evaluated for minimum seasonal air temperature and maximum daily air temperature rise in winter. Evaluating data from 31 seasons, the method of ISO13793 (2001) is used to determine the values for the 10-year recurrence interval. An empirical curve is fitted to the scattered relationship between these values and the FI_{10} at the respective locations of many reservoirs. Thereafter, a FI_{10} is selected, ice thickness is determined from an expression from the literature, and minimum air temperature and maximum air temperature rise are taken from above correlations. A thermal ice model

is initialized with an equilibrium ice temperature profile corresponding to the minimum air temperature and ice thickness, and then exposed to a sudden air temperature increase. The ice temperature development is simulated in response to this air temperature increase, and from this the ice stress development throughout the depth of the ice is calculated. The ice stress is integrated through the thickness of the ice to determine the peak thermal line load from this air temperature rise. This is taken as the design line load corresponding to the originally selected FI_{10} . The calculation is performed over a range of FI_{10} , and the resulting design loads are fitted to an empirical curve. This curve happens to be similar to the relationship for the 50-year design load of the probabilistic model.

1.3.3 Explicit Equation

The deterministic model is simplified by approximating ice temperature and ice temperature rise at one characteristic depth in the ice cover, and the rheological model is reduced to an explicit relationship between ice temperature rise and peak stress. The design line load is obtained by multiplying that peak stress with the ice thickness. The equation can be solved explicitly for the input relationships of the deterministic model, providing an expression for design line load as a function of FI_{10} . It turns out that this expression predicts that the design line load is proportional to the ice thickness. This relationship can indeed be used to fit the result of the probabilistic model.

1.3.4 Snow

The ice in this study has been assumed to be covered by a “thin snow cover”, defined as a snow cover that produces an ice cover of thickness

$$H_{ice} = 0.02 FI^{0.5}, \quad (1.5)$$

where H_{ice} is in m and FI in °C days. An equation like this is stated in NVE (2003) and was presumably taken from the work of Carter et al. (1998). Hence, a snow depth algorithm first had to be devised that made the energy conserving ice growth model reproduce this ice thickness. The Deterministic Model used this ice thickness expression directly and made a simple assumptions for the snow depth at the time of peak ice loads that is slightly different from the snow depth algorithm of the Probabilistic Model. The Explicit Equation is based on the same assumptions as the Deterministic Model.

While an attempt was made in this study to compare snow depth and ice thickness observations from the NVE Varsom Regobs database (<https://www.regobs.no/>) with the local Freezing Index, this effort was ultimately aborted due to the need of quality controlling the reported observations.

Chapter 2

Materials and Methods

2.1 Temperature

The climate of Norway comprises of three groups under the Köppen climate classification system: C (temperate), D (continental), and E (polar), i.e. encompassing regions where the monthly average temperature is always above 0 °C (C) to regions where it is always below 10 °C (E). Elevation ranges from sealevel to over 2400 m, and the topography is often steep with an abundance of spectacular fjord. Although these features make temperature interpolation challenging, NVE provides operational interpolation of air temperature observations from MET Norway's Climate Databases (KDVH) onto a 1 km grid throughout the country. Data are updated daily and go as far back as the beginning of 1957. Daily average temperatures are distributed under the brand name seNorge (<https://www.senorge.no/>), and the current data version 2 (v2) forms the basis for this study (Lussana et al., 2016). The product is regarded as an unbiased estimator for air temperatures above -30 °C. At temperatures below -30 °C, interpolated air temperatures have been found to show a systematic warm bias (Lussana et al., 2016). When obtaining temperature data for specific reservoirs spanning several seNorge grid cells, the grid cell was chosen with an elevation closest to the high-water line of the reservoirs. Temperature data from seNorge v2 were used without further processing.

The aim of this study is to predict thermal line loads in terms of readily available metrics of a location. While it is common to describe ice formation in terms of freezing degree days (FDD), i.e. the cumulative sum of daily sub-zero air temperature, this metric is not readily available to the practitioner in Norway. Instead, the Norwegian Public Roads Administration (SVV) distributes a gridded Freezing Index (FI) product based on seNorge data (Kvande et al., 2023). The seasonal Freezing Index is the average temperature of the freezing season times the length of the freezing season. The freezing season is the period of time with mostly sub-zero temperatures. The mathematical definition of the freezing period is given in ISO13793 (2001) and the implementation used in this study is described below. The FI is identical to the FDD if the air temperature drops below and stays below zero at one time in fall and rises above and then stays above zero at one time in spring. Otherwise, $FI < FDD$, and the more days appear above zero air temperature during the winter, the bigger the difference between FI and FDD. Incidentally, it turned out during this study that the FI is a better metric to describe the output of ice growth models in Norway than the FDD (Section 3.1). As of writing, a convenient user interface is available with a browsable map (<https://www.vegvesen.no/kart/visning/frostsonerkart>), presenting the Freezing Index for 10 year (FI_{10}) and 100 year recurrence (FI_{100}). The 10-year and 100-year values were determined from a Gumbel distribution fitted to annual FI data. The procedure and definition of the Freezing Index are described in ISO13793 (2001). The data currently presented by SVV are based on temperatures from the climate normal 1991–2020. However, as of writing, the SVV map is based mostly on seNorge v1 data with the last three years from seNorge v2 (Helga Therese Tilley Tajet, personal communications, May 2023). A preliminary investigation performed as part of the current study showed that the difference between the FI_{10} from SVV and FI_{10} calculated entirely from seNorge v2 data may be as high as $\pm 20\%$ locally.

Petrich and Arntsen (2018) used the full seNorge air temperature record since 1957 to calculate thermal

ice loads. They detrended the determined line loads in order to make statements about the state “today”. However, after a brief investigation of air temperature data from the 20th Century Reanalysis v3 (20CRv3), it was decided that it would be preferred to use data of the period 1991–2020 without detrending in this study as this is a standard procedure that results in consistency with the WMO Climatological Normal period 1991–2020. While the climate normal is comprised of 30 calendar years, this study uses 31 winters (1990/91 to 2020/21, inclusive) to avoid partial winter seasons.

2.2 Calculation of the Freezing Index

Freezing Degree Days (FDD) are defined as

$$FDD = \sum \Delta t \begin{cases} -\theta & \text{for } \theta < 0^\circ\text{C}, \\ 0 & \text{else,} \end{cases} \quad (2.1)$$

where the sum is calculated from the beginning of winter until the date of interest, θ is the air temperature and Δt is the period of time over which the air temperature is valid. While Freezing Degree Days (FDD) are trivial to calculate for any day during the winter season, the Freezing Index (FI) is defined in ISO13793 (2001) only as an aggregate metric for an entire, reasonably cold winter season. Challenges in the automated determination of the FI were recognized early in the history of automated data processing (Straub & Wegmann, 1965). According to ISO13793 (2001), the freezing index can be calculated as the difference between the cumulative air temperature maximum and minimum during a winter season. This is recognizing that there will be a point in time in fall after which the air temperatures are predominantly negative and hence the cumulative air temperature will mostly decrease from this time onward. This marks the onset of the freezing season. Likewise, at some point in spring air temperatures will become predominantly positive after which the cumulative air temperature will start to reasonably consistently increase. This marks the end of the freezing season. At least two practical issues arise:

1. How is the FI to be calculated for a particular day of the season?
2. In a temperature time series with only occasional temperature excursions below zero, what is an efficient algorithm to identify the relevant maximum and minimum?

In this study, the Freezing Index for either a season or a certain point in time is calculated from the temperature record starting the preceding 1 August until the date of interest (or the end of the season, e.g. 31 July the following year).

1. Within that temperature record, the (latest) date of occurrence of the lowest temperature is identified, and the (latest) date of the coldest 3-day period is identified. The later one of these two is chosen as a separation point.
2. The date of highest cumulative temperature occurring before the separation point is taken as the initial date.
3. The date of the lowest cumulative temperature occurring on or after the separation point is taken as the final date.
4. The difference in cumulative temperature between the initial date and the final date is the Freezing Index.

2.3 Rheological Model of Thermal Ice Loads

The rheological model used in this study had been described by Petrich and Arntsen (2018). It is driven by ice temperature derived from either the probabilistic model, deterministic model, or the explicit equation.

The time history of ice stress was calculated at each vertical level of the ice growth model. The rheological model of Bergdahl (1978) and Cox (1984) was used with parameters discussed by Petrich et al. (2015). Ice stress was calculated from

$$\frac{d\sigma}{dt} = A \frac{dT}{dt} - B \left(\frac{T_0}{T} \right)^m \left(\frac{\sigma}{\sigma_0} \right)^n, \quad (2.2)$$

where σ is the local stress (positive in compression, with an extension to negative stresses as described by Petrich et al. (2015)), T is the local ice temperature, $A = 200 \text{ kPa/K}$ is the product of the relevant linear elastic modulus (cf. Cox (1984) for a discussion) and linear thermal expansion of the ice, $B = 342 \text{ kPa/day}$ is the product of the elastic modulus and a constant describing creep of ice, $m = 1.92$ and $n = 3.7$ are fitted constants, and $T_0 = -1 \text{ }^\circ\text{C}$ and $\sigma_0 = 100 \text{ kPa}$ are constants for dimensional scaling. The ice temperature record from the thermal model was used to derive input parameters dT/dt and T , and the non-linear equation was solved implicitly at each time step, i.e. the solution for σ^i at time step i was determined numerically from the value σ^{i-1} one time step Δt earlier by iteratively solving

$$\sigma^i = \sigma^{i-1} + A (T^i - T^{i-1}) - B \left(\frac{T_0}{\min\{T_{\max}, \frac{1}{2}(T^i + T^{i-1})\}} \right)^m \frac{1}{2} \left[\left(\frac{\sigma^i}{\sigma_0} \right)^n + \left(\frac{\sigma^{i-1}}{\sigma_0} \right)^n \right] \quad (2.3)$$

for σ^i . The stress σ^i was set to 0 whenever $T^i \geq 0 \text{ }^\circ\text{C}$, the limit $T_{\max} = -0.001 \text{ }^\circ\text{C}$ is introduced for numerical reasons, and $\min\{a, b\}$ is the minimum operator that returns the lesser of a and b . A zero-crossing from σ^{i-1} to σ^i was prevented if the sign of dT/dt rendered this unphysical, i.e., σ^i was set to 0 in that case. Ice fracture in tension or compression was not treated explicitly (i.e., calculation was performed as in Petrich and Arntsen (2018) and unlike Côté et al. (2016) or Petrich et al. (2020)).

At each time step, the line load was calculated from the vertical stress profile according to

$$LL^i = \sum_{j=1}^{N_z} \sigma_j^i (1 - \phi_j^i) \Delta z, \quad (2.4)$$

where LL^i is the line load at time step i , N_z is the number of cells in the discretized column, Δz is the cell height, ϕ_j^i is the liquid volume fraction in cell j at time step i , and σ_j^i is the stress at cell j at time step i .

2.4 Model of Ice Growth and Ice Temperature

The ice growth model is a one-dimensional enthalpy-conserving heat transfer model (a column model) that treats phase change based on the enthalpy-porosity approach (e.g. Brent et al., 1988; Petrich et al., 2006). Ice grows or melts in response to the temperature profile in ice and water, which in turn changes in response to changes of the air temperature (and snow cover). This model starts with a water column of $4 \text{ }^\circ\text{C}$ on 1 August of each year and then adds or removes heat at the air-water surface depending on air temperature. If the water temperature falls below $0 \text{ }^\circ\text{C}$ ice is formed instead. Subsequent changes of the air temperature will change the ice temperature near the upper surface, and heat will be conducted through the water and ice accordingly. This changes the temperature profile through the ice, which can be used to calculate thermal stresses. Whenever the temperature at the ice-water interface falls below 0, ice is formed. When the temperature at the ice-water interface increases above 0, ice is melted. The key feature is that this model inseparably links the temperature profile of the ice to ice growth and melt, i.e. ice temperature and thickness are mutually dependent on each other, which is implied by “enthalpy-conserving”.

Unlike the model Petrich and Arntsen (2018), the open water treatment for large reservoirs was removed, and the ice is snow-covered in a manner that generates the ice thickness equation of NVE (2003) (Equation 1.2). While Equation 1.2 was originally intended to be used to predict the ice thickness based on the freezing degree days of a winter season, NVE (2003) re-interprets this by referring to 100-year tabulated frost data, which is actually a Freezing Index (FI). In regions growing only a thin ice cover, Equation 1.2 is unlikely to be successful if used with FDD and should rather be used with FI to account for air temperatures alternating between both sides of 0°C throughout the winter (cf. Section 3.1). Hence, a description of the air-ice heat transfer coefficient, h , had to be sought that makes the ice growth model (Section 2.4) grow ice with a maximum ice thickness H_{max} in a winter with Freezing Index FI ,

$$H_{max} = 0.02 FI^{0.5}, \quad (2.5)$$

where H_{max} is in m and FI in $^\circ\text{C}$ days. The method used for this was trial-and-error until a description was found with physically reasonable parameters that was as simple as possible.

It follows a more detailed description of the ice growth model and its implementation in Section 2.4.1.

2.4.1 Model Implementation

The energy conservation equation solved is

$$\bar{c}\rho \frac{dT}{dt} = \frac{d}{dz} \bar{k} \frac{dT}{dz} - L\rho \frac{d\phi}{dt} + S. \quad (2.6)$$

This equation was discretized in a vertical column of grid cells with a uniform height Δz using the Finite Volume Method (FVM) as laid out by Patankar (1980) and solved implicitly. A fully implicit formulation was chosen to avoid artificial temperature oscillations in the presence of large time steps. The tridiagonal matrix equation was solved by LU factorization exposed by SciPy (Virtanen et al., 2020).

In the following, the numerical vertical cell position is denoted j , where j increases downward, while the physical vertical coordinate z increases upward. Starting at time step $i - 1$, the cell temperature T at time step i is determined from the fully implicit equation

$$\frac{\bar{c}\rho_j^*}{\Delta t} T_j^i - \frac{\bar{c}\rho_j^{i-1}}{\Delta t} T_j^{i-1} = 2 \left(\frac{1}{\bar{k}_{j-1}^*} + \frac{1}{\bar{k}_j^*} \right)^{-1} \frac{T_{j-1}^i - T_j^i}{(\Delta z)^2} - 2 \left(\frac{1}{\bar{k}_j^*} + \frac{1}{\bar{k}_{j+1}^*} \right)^{-1} \frac{T_j^i - T_{j+1}^i}{(\Delta z)^2} - L\rho \frac{\phi_j^* - \phi_j^{i-1}}{\Delta t} + S_j^*, \quad (2.7)$$

where the starred parameters (*) are based on the currently best estimate for T^i and ϕ^i . Initially, the starred parameters are set to T^{i-1} and ϕ^{i-1} . A phase fraction correction

$$\Delta\phi_j^* = \max \left\{ -\phi_j^*, \min \left\{ 1 - \phi_j^*, \frac{\bar{c}\rho_j^* T_j^i}{L\rho} \right\} \right\} \quad (2.8)$$

is calculated to account for freezing or melting (the functions $\min\{a, b\}$ and $\max\{a, b\}$ return the lesser and the greater of a and b , respectively). The correction $\Delta\phi_j^*$ is added to ϕ_j^* , then $\bar{c}\rho_j^*$ and \bar{k}_j^* are updated based on the new ϕ_j^* , and Equation 2.7 is solved again. This is repeated until $\Delta\phi_j^* \leq 10^{-6}$ everywhere in the computational domain. At that point the current ϕ_j^* becomes ϕ_j^i (i.e., $\phi_j^i := \phi_j^*$) and the calculation of time step i is finished.

In the energy conservation equation 2.6, S is a source term that is non-zero in the current model only at the upper ("top") and lower ("bottom") boundaries of the numerical domain, t is time, z is distance along the vertical axis, $L = 334 \text{ kJ/kg}$ is the latent heat of fusion of ice, $\rho = 920 \text{ kg/m}^3$ is the density of ice, ϕ is the local liquid volume fraction (or the grid cell average in Equation 2.7), T is the local temperature of ice or water

(or the grid cell average in Equation 2.7), and the thermodynamic properties at each location or within each grid cell are

$$\bar{c}_p = c_w \rho_w \phi + c_j \rho_j (1 - \phi), \quad (2.9)$$

where $c_w = 4200 \text{ J}/(\text{kg K})$ and $c_j = 2100 \text{ J}/(\text{kg K})$ is the specific heat capacity of water and ice, respectively, $\rho_w = 1000 \text{ kg}/\text{m}^3$ and $\rho_j = 920 \text{ kg}/\text{m}^3$ is the density of water and ice, respectively, and

$$\bar{k} = k_w \phi + k_j (1 - \phi), \quad (2.10)$$

where $k_w = 0.56 \text{ W}/(\text{m K})$ and $k_j = 2.0 \text{ W}/(\text{m K})$ are the thermal conductivity of water and ice, respectively. In cells that are neither completely solid nor completely liquid, i.e. $0 < \phi < 1$, the liquid phase fraction ϕ is iteratively adjusted to maintain $T = 0^\circ \text{C}$ at each time (Equation 2.8).

The first (second) term on the right-hand-side of Equation 2.7 is not defined at the upper (lower) boundary of the domain because it contains a reference to the cell above (below) the upper-most (lower-most) cell, j . Hence, is removed from the equation describing the boundary cell and any heat exchange through the interface is expressed through the source term S_j^* .

The lower boundary of the domain provides a constant heat flux of $F = 2 \text{ W}/\text{m}^2$ into the water. Hence

$$S_{bottom}^* = \frac{F}{\Delta z}, \quad (2.11)$$

where Δz is the vertical size of the numerical cell, and the second term on the right-hand-side of Equation 2.7 is omitted.

The heat flux at the upper boundary is determined implicitly through Newton's law of heat transfer from the prescribed air temperature at time step $i - 1$, T_{air}^{i-1} , the temperature of the cell at the upper surface, and the thermal resistance imposed by the thermal conductivity of the surface cell in series with an ice-air heat transfer coefficient h . It is

$$S_{top}^* = \frac{T_{air}^{i-1} - T^i}{\Delta z} \left[\frac{1}{h} + \frac{\Delta z}{2k} \right]^{-1} \quad (2.12)$$

and the first term on the right-hand-side of Equation 2.7 is omitted. The heat transfer coefficient is $h = 15 \text{ W}/(\text{m}^2 \text{ K})$ for snow-free and windy conditions, and a function of ice thickness H (Equation 2.13), defined in Section 3.3.1 for snow-covered conditions. If the snow cover depends on ice thickness, then h is updated once at the start of the numerical time step based on ice thickness at time step $i - 1$, i.e. based on H^{i-1} .

With only a moderate bottom heat flux F , melt is typically dominated by surface ablation.

Surface ablation is treated as follows: each time step the upper-most cell is completely liquid ($\phi = 1$) while lower-lying cells still contain ice ($\phi < 1$), the ice is made to float up to the surface. This was implemented as a copy operation of the porosity and temperature fields of the domain "upward" by one cell. Since the thermal conductivity of water is less than the conductivity of ice, the rate of surface ablation may be underestimated.

The ice thickness H at time step i was calculated from

$$H^i = \sum_{j=1}^{N_z} \phi_j^i \Delta z \quad (2.13)$$

and the maximum ice thickness of the season was used later in the analysis.

The domain was 15 m high with grid size $\Delta z = 0.1 \text{ m}$, initial conditions were $\phi = 1$ and $T = 4^\circ \text{C}$ on 1 August of each year, and the time step was $\Delta t = 86400 \text{ s}$ (1 day), corresponding to the air temperature record. The energy conservation equation was solved implicitly. Since the model did not include melt from solar radiation it was expected that melt rates were underestimated in summer. Simulations were performed separately for each season, i.e. from 1 August until 31 July of the following year. Hence, perennial ice was not able to form.

2.5 Peak Ice Load Probability Distribution

A manual pre-screening of probability distribution functions and methods for parameter estimation was performed based on the comments in Section 1.2.2. Simulations of annual peak line loads were inspected from a set of approximately 30 reservoirs from different regions of Norway that included reservoirs of insignificant line loads in some years (< 1 kN/m) and reservoirs with modeled peak line loads exceeding 150 kN/m in snow-covered conditions. The result of this clearly favored the use of the Normal Distribution with the Probability Paper Method, which allowed for the treatment of line loads < 1 kN/m as nondetects. A quantitative test (e.g. χ^2 -test) was not performed due to the small sample size of only 30 winters per reservoir.

The probability distributions are shown in the Results Section 3.3.3. Distributions were fitted to Normal, Log-Normal, and Gumbel and Generalized Extreme Value distributions with the Probability Paper Method, Method of Moments, L-Moments, and Maximum Likelihood Estimator.

The annual peak thermal line load was determined for each reservoir location from simulations of 31 winters. For each reservoir separately, the Normal Distribution was fitted with the Probability Plot Method (Equation 1.3), i.e. by scaling the axes and performing a linear least squares fit. Winters without ice or with peak thermal line loads < 1 kN/m were treated as nondetects and are not used for fitting but affect the plotting position of the remaining data. Once the probability distribution was found for a given reservoir, the 50-year peak thermal line load was the 98-percentile of the cumulative distribution function.

There are at least two ways to perform the Probability Plot parameter estimation mathematically: either by performing two least square fits and combining them (e.g. Gumbel, 1954; Gumbel, 1958), or by pre-calculating reduced parameters for the desired number of observations and return period, and scaling mean and standard deviation of the dataset accordingly (e.g. ISO13793, 2001). The reduced parameters depend on the number of nondetects in the dataset. The parameter estimation for the first method is outlined in Algorithm 1 (Gumbel, 1954, pp. 15 - 16). Once the parameters μ and either σ or β of the distribution are known, the line load of return period n can be calculated as

$$LL_n = \mu + \sigma\sqrt{2} \operatorname{erf}^{-1} \left(2\frac{n-1}{n} - 1 \right) \quad (2.14)$$

for the Normal Distribution, or

$$LL_n = \mu + \beta \left[-\ln \left(-\ln \frac{n-1}{n} \right) \right] \quad (2.15)$$

for the Gumbel Distribution.

Algorithm 1: Calculation of Probability Distribution Parameters using the Probability Plot Method

- 1 Let m be the number of observations (30 in our case), n the sought return period (50 in our case), and d the number of winters without ice loads (i.e. nondetects).
 - 2 Let w_i with $i = 1 \dots m - d$ be the observed values without nondetects ordered from smallest value to largest value.
 - 3 Let $u_i = (i + d)/(m + 1)$ with $i = 1 \dots m - d$ be the rank order numbers.
 - 4 Let $v_i = -\ln(-\ln u_i)$ and $v_i = \sqrt{2} \operatorname{erf}^{-1}(2u_i - 1)$ for Gumbel and Normal Distribution, respectively.
 - 5 Perform a least-squares fit $w = a_0v + b_0$ for parameters a_0 and b_0 .
 - 6 Perform a least-squares fit $v = a_1w + b_1$ for parameters a_1 and b_1 .
 - 7 The parameters of the distribution are $\mu = \left| \frac{b_0b_1}{a_1} \right|^{0.5}$ and $\sigma = \left(\frac{a_0}{a_1} \right)^{0.5}$ for the Normal Distribution. For the Gumbel Distribution the second parameter is conventionally called β rather than σ .
-

Another option is to determine the design line load from an equation similar to the one given in ISO13793



(2001). Adapting the notation of ISO13793 (2001),

$$LL_n = \overline{LL} + s_{LL} \frac{y_n - \bar{y}}{s_y}, \quad (2.16)$$

where \overline{LL} and s_{LL} are calculated from all observations but the nondetects according to

$$\overline{LL} = \frac{1}{m-d} \sum_{i=1}^{m-d} LL_i, \quad (2.17)$$

$$s_{LL} = \sqrt{\frac{1}{m-d} \sum_{i=1}^{m-d} (LL_i - \overline{LL})^2}, \quad (2.18)$$

and y_n , \bar{y} and s_y were pre-calculated according to Gumbel (1954). Representative results of the calculation for the parameters of interest in this study are given in Table 2.1. Here, $m = 30$ is the number of observations, d is the number of observed nondetects, and $n = 50$ is the return period sought. Note that for mathematical correctness, Equation 2.18 needs to define the population standard deviation (i.e., dividing by $m - d$) (Gumbel, 1954) rather than the sample standard deviation (i.e., dividing by $m - d - 1$) (Gumbel, 1958; ISO13793, 2001). Hence, the parameters of the distribution (Equations 2.14 and 2.15) are

$$\mu = \overline{LL} - \frac{s_{LL}}{s_y} \bar{y} \quad \text{and} \quad (2.19)$$

$$\sigma = \frac{s_{LL}}{s_y} \quad (2.20)$$

for the Normal Distribution, while the parameter in Equations 2.20 would be called β rather than σ for the Gumbel Distribution.

2.6 Probabalistic Model

The probabalistic ice load model is relatively simple. At each reservoir location and for each winter of the 30-year record considered, the air temperature record was used (Section 2.1) to drive the ice growth model (Section 2.4), which was then used to derive the peak line load for each winter season (Section 2.3). Based on the annual peak line loads from that 30-year record, the parameters of the probability distribution were determined individually for each location and the line load with 50-year recurrence rate, LL_{50} , was calculated (Section 2.5). The 10-year Freezing Index FI_{10} was calculated from the air temperature data (Section 2.2). Using the LL_{50} and FI_{10} data of all locations, a straight line was fitted on a log-log plot to relate LL_{50} to FI_{10} . Since gridded data of FI_{10} are available for Norway, the design line load LL_{50} can be determined with ease at any location.

2.7 Air Temperature Characteristics

Thermal ice loads are brought about by a change in ice temperature, moderated by an ice-temperature dependent creep rate. Generally, high rates of temperature increase combined with low ice temperatures will result in higher ice loads. Ice temperatures depend on air temperature, and hence the typical (i.e. 10-year rate of recurrence) minimum air temperature and typical winter-time rate of air temperature change for a given location shall be determined from seNorge data. Temperature rise was defined as the increase in daily air temperature from one day to the next, where the next day's temperature is capped at an upper limit of 0 °C (i.e. an increase from -5 °C on one day to either 0 or 1 °C the next day would have been counted as a $\Delta\theta = 5$ °C temperature rise).

Table 2.1: Parameters for Equation 2.16

m	d	n	Gumbel Distribution			Normal Distribution		
			y_n	\bar{y}	s_y	y_n	\bar{y}	s_y
10	0	50	3.90	0.50	0.95	2.05	0.00	0.79
20	0	50	3.90	0.52	1.06	2.05	0.00	0.87
30	0	50	3.90	0.54	1.11	2.05	0.00	0.90
30	1	50	3.90	0.60	1.08	2.05	0.06	0.85
30	2	50	3.90	0.65	1.06	2.05	0.12	0.81
30	3	50	3.90	0.71	1.03	2.05	0.17	0.77
30	4	50	3.90	0.77	1.01	2.05	0.22	0.74
30	5	50	3.90	0.82	1.00	2.05	0.27	0.72
30	6	50	3.90	0.87	0.98	2.05	0.32	0.69
30	7	50	3.90	0.93	0.96	2.05	0.37	0.67
30	8	50	3.90	0.99	0.95	2.05	0.41	0.65
30	9	50	3.90	1.04	0.93	2.05	0.46	0.63
30	10	50	3.90	1.10	0.92	2.05	0.50	0.61
30	0	100	4.60	0.54	1.11	2.33	0.00	0.90
31	0	50	3.90	0.54	1.12	2.05	0.00	0.90
40	0	50	3.90	0.55	1.14	2.05	0.00	0.92
50	0	50	3.90	0.55	1.16	2.05	0.00	0.93

The minimum air temperature, θ_0 , and maximum air temperature rise, $\Delta\theta$, were determined for 31 winter seasons at selected locations. The distribution was fitted to a Gumbel distribution following ISO13793 (2001) and the 10-year rate of recurrence was determined. The scattered data were linearly fitted on a log–log plot.

2.8 Deterministic Model

An undeformed slab of ice is considered of homogeneous physical properties from top to bottom. Thermal ice loads are generated when the ice temperature increases. The magnitude of the thermal loads at a given time depends on (a) the thickness of the ice, (b) the (recent history of the) rate of change of ice temperature, (c) the ice temperature. While (a) depends on air temperature and snow cover in the past weeks or months, (b) and (c) depend on air temperature and snow cover at the time of the event. In this deterministic model, the peak-load-generating event at a location characterized by a particular value of FI_{10} is generated in an ice cover of thickness

$$H = 0.02 \text{ m } FI_{10}^{0.5} \quad (2.21)$$

that started in a stress-free state with a linear temperature gradient in the ice corresponding to a 10-year minimum air temperature according to Section 2.7 and was then subjected to a 10-year air temperature rise according to Section 2.7. The time step of the temperature model was 1 day.

Two scenarios are considered in the deterministic model: (I) snow-free, and (II) moderate snow load. Moderate snow load is defined as a snow load that does not yet result in negative freeboard. Further, three degrees of severity are defined: the reference case, “low”, and “high”, where low and high are the conditions leading to lower and higher thermal ice loads, respectively. The parameters for these scenarios are defined in Table 2.2. The model proceeds as follows:

1. FI_{10} is used to calculate separately
 - (a) the maximum ice thickness of the winter season,

Table 2.2: Constants and equations defining the Deterministic Model. In the equations, FI_{10} is the 10-year Frost Index in multiples of 1 °C days, H_{ice} is the ice thickness in m, and the units of coefficients c_1 and c_2 are such that the corresponding equation is dimensionally correct. Sensitivity of line load to the parameters is shown separately for Scenarios I and II.

Step	Symbol	Unit	Scenario	Equation	Constants, or Coefficients c_1 and c_2			Sensitivity	
					Reference	Low	High	I	II
1.a.I	H_{ice}	m	I	$c_1 FI_{10}^2$	0.01, 0.64	0.009, 0.64	0.011, 0.64	7%	
1.a.II	H_{ice}	m	II	$c_1 FI_{10}^2$	0.02, 0.5	0.018, 0.5	0.022, 0.5		11%
1.b	$\Delta\theta$	°C	I & II	$c_1 FI_{10}^2$	1.05, 0.348	0.924, 0.348	1.18, 0.348	3%	4%
1.c	θ_0	°C	I & II	$c_1 FI_{10}^2$	-1.38, 0.406	-1.24, 0.406	-1.52, 0.406	7%	6%
2.I	h	W/(m ² K)	I		17	15.3	18.7	1%	
2.II	h	W/(m ² K)	II	$(1/c_1 + c_2 H_{ice})^{-1}$	17, 0.5	15.3, 0.55	18.7, 0.45		5%
3	Δz	m	I & II		0.005			<1%	<1%
	Δt	s			3600				
3	ρ_i	kg/m ³	I & II		920			< 3%	< 3%
	c_i	J/(kg K)			2100				
	k_i	W/(m K)			2				
4	A	kPa/K	I & II		200	180	220	6%	6%
	B	kPa/day			342	376	307		
	n	-			3.7	3.7	3.7		
	m	-			1.92	1.92	1.92		
	T_1	°C			-1	-1	-1		
	σ_0	kPa			100	100	100		

- (b) the 10-year maximum increase of daily average air temperature (below the freezing point), and
(c) the 10-year minimum air temperature (Section 2.7, resulting parameters in Table 2.2).

- A heat transfer coefficient from air through snow into the ice is determined to calculate the ice temperature profile. For load events in the absence of snow (I) the heat transfer coefficient is a constant, and for load events in the presence of a surface snow cover (II) the heat transfer coefficient depends on snow depth which is assumed to be proportional to ice thickness (Table 2.2).
- A transient vertical ice temperature profile is calculated through a slab of thickness according to Item 1a. The bottom of the ice is at its freezing point at 0 °C, and heat transfer from the air is determined by the heat transfer coefficient for scenario (I) or (II). The calculations are initiated with a linear temperature profile consistent with the minimum air temperature (Item 1c), with air temperature instantaneously raised according to (Item 1b). Physical parameters of the model are given in Table 2.2.
- Finally, a vertical ice stress profile is calculated from the temperature profile and integrated over the thickness of the ice. This method is based on earlier work with parameters given in Table 2.2 (Petrich et al., 2015; Petrich & Arntsen, 2018).

2.9 Explicit Equation

There is no closed form solution to the transient ice temperature and stress that would allow for an explicit solution of Steps 3 and 4 in Section 2.8 rather than numerical modeling. However, there is precedent in attempting to reduce the temperature development in the ice to a single rate of temperature change and relating this to the peak line load. Such efforts date back at least to the work of Royen in 1922 (Bergdahl, 1978), and a more recent example would be the work of Fransson (1988). Although the numerical solution of Steps 3

and 4 presents no computational challenges, this section adds to this body of work with the development of an explicit approach suitable for environmental parameters relevant to the Deterministic Model. The explicit approach is used in this study to give physically-based support for the choice of a best-fit equation.

This Section presents a method that can be used to estimate thermal ice loads resulting from a step-change in air temperature. The thermal line load (LL) is the vertical stress profile of the ice integrated over the thickness of the ice. Here, this integral is simplified to a representative stress (σ_r) multiplied by the thickness of the ice (H_{ice}), i.e.

$$LL = \sigma_r H_{ice} \tag{2.22}$$

where the ice thickness is specified, and the representative stress during a load peak is calculated from the rheological model (Equation 2.2) by recognizing that the rate of change of stress $d\sigma/dt = 0$. I.e.,

$$\sigma_r = \sigma_0 \left[\frac{A}{B} \frac{\Delta T}{\Delta t} \left(\frac{T_r}{T_1} \right)^m \right]^{\frac{1}{n}}, \tag{2.23}$$

where $\Delta T/\Delta t$ is the rate of change in ice temperature, the remaining coefficients are from Petrich et al. (2015) (cf. Table 2.2), and care is taken to use consistent dimensions of time (B uses days). This equation is valid if the peak stress is reached while the temperature is still increasing. Noting that the bottom of the ice is at 0°C , the increase of ice temperature, ΔT , is related to the increase in air temperature, $\Delta\theta$, through

$$\Delta T = \frac{\Delta\theta}{\theta_0} T_0, \tag{2.24}$$

where θ_0 and T_0 are the initial temperature of the air and ice, respectively. The characteristic time required for this change is

$$\Delta t = \left(\frac{H_{ice}}{2} \right)^2 \frac{\rho_i c_i}{k_i}, \tag{2.25}$$

where ρ_i , c_i , and k_i are density, heat capacity, and thermal conductivity of the ice, respectively. The initial temperature at the center of the ice is

$$T_0 = \frac{1}{2} \frac{\theta_0}{1 + \frac{k_i}{hH_{ice}}}, \tag{2.26}$$

where h is the heat transfer coefficient from air through snow into ice. The representative temperature during the step change is

$$T_r = T_0 + \alpha_d \Delta T, \tag{2.27}$$

where $\alpha_d = 1.0$ is an empirical mixing coefficient appropriate for the model parameters (Table 2.2). Hence, the peak line load can be written as an explicit expression,

$$LL = H_{ice} \sigma_0 \left[\frac{A}{B} \frac{\Delta T}{\Delta t} \left(\frac{T_r}{T_1} \right)^m \right]^{\frac{1}{n}}, \tag{2.28}$$

$$= H_{ice} \sigma_0 \left[\frac{A}{B} \frac{\Delta\theta}{\theta_0} \frac{1}{2} \frac{\theta_0}{1 + \frac{k_i}{hH_{ice}}} \frac{4k_i}{\rho_i c_i} \frac{1}{H_{ice}^2} \left(\frac{1}{T_1} \frac{1}{2} \frac{\theta_0}{1 + \frac{k_i}{hH_{ice}}} \left\{ 1 + \alpha_d \frac{\Delta\theta}{\theta_0} \right\} \right)^m \right]^{\frac{1}{n}}, \tag{2.29}$$

$$= H_{ice} \sigma_0 \left[\frac{A}{B} \frac{2k_i}{\rho_i c_i} \frac{\Delta\theta}{1 + \frac{k_i}{hH_{ice}}} \frac{1}{H_{ice}^2} \left(\frac{1}{2T_1} \frac{\theta_0}{1 + \frac{k_i}{hH_{ice}}} \left\{ 1 + \alpha_d \frac{\Delta\theta}{\theta_0} \right\} \right)^m \right]^{\frac{1}{n}}. \tag{2.30}$$

Chapter 3

Results

3.1 Freezing Index versus Freezing Degree Days

While ice thickness is typically described as a function of Freezing Degree Days (FDD), the frequent wintertime air temperature excursions above the freezing point in the coastal regions of Norway would suggest that FDD may not be the most suitable metric to describe ice growth throughout Norway. Figure 3.1 shows the seasonal maximum ice thickness (H_{max}) derived from the ice growth model with the snow parameterization of the

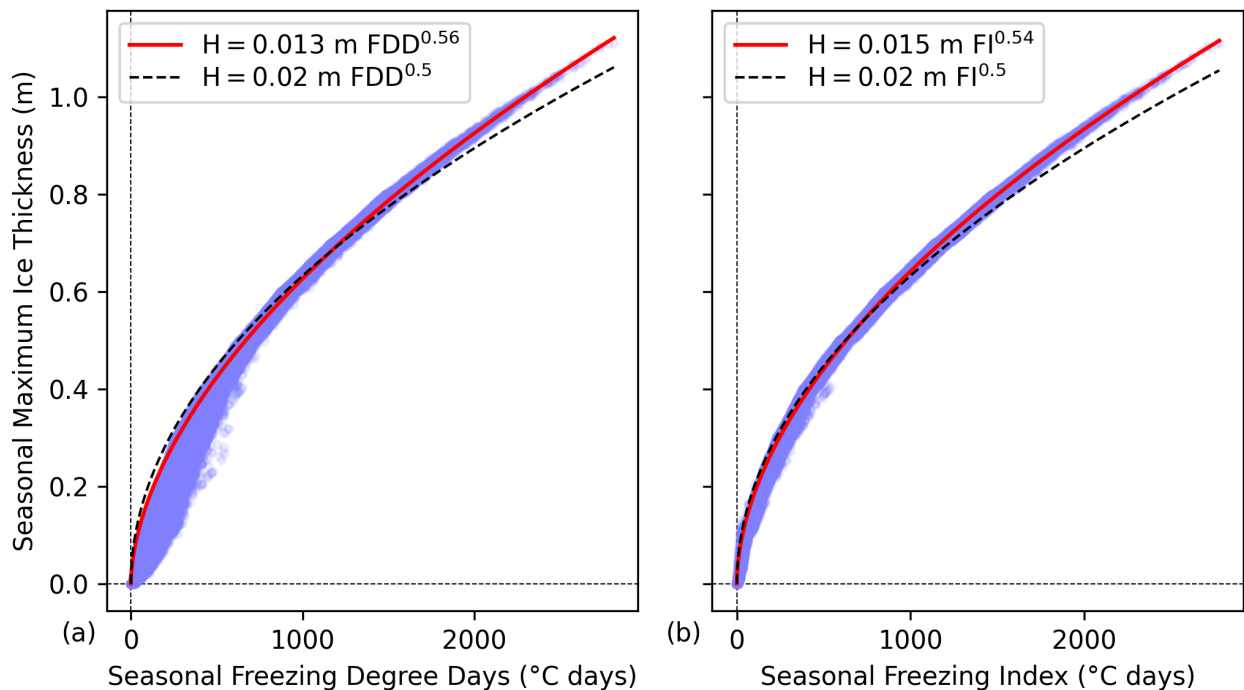


Figure 3.1: Seasonal maximum ice thickness vs seasonal maximum (a) Freezing Degree Days and (b) Freezing Index from simulations at 2696 reservoirs over 31 winters.

probabilistic model (Equation 3.5) depending on the seasonal maximum Freezing Degree Days (Figure 3.1a) and Freezing Index (Figure 3.1b). By design, the data approximate a curve that resemble the target functions

Equations 3.1 and 3.2, respectively,

$$H_{max} = 0.02\sqrt{FDD_{max}}, \quad \text{and} \quad (3.1)$$

$$H_{max} = 0.02\sqrt{FI_{max}}, \quad (3.2)$$

where H_{max} is in m, and FDD_{max} and FI_{max} are in multiples of $^{\circ}\text{C}$ days. The Freezing Index-based relationship shows considerably less scatter below 700°C days (Figure 3.1b), suggesting that Equation 3.2 is a better proxy for ice thickness throughout mainland Norway than Freezing Degree Days.

3.2 Genesis of a Thermal Ice Load Event

The development of a thermal line load peak from the combination of the temperature model and the rheological model of Sections 2.4 and 2.3 shall be illustrated in this section.

In linear systems the response can be calculated from a superposition of input step functions. This is not the case for thermal ice loads due to the non-linear relationship between air temperature and ice thickness, air temperature change and ice temperature change, and ice temperature change and stress. The latter two aspects are illustrated in Figure 3.2 by showing the line load response of an ice cover to a sudden change in air temperature. An ice cover had been grown at an air temperature of $\theta = -15^{\circ}\text{C}$. After two months, the

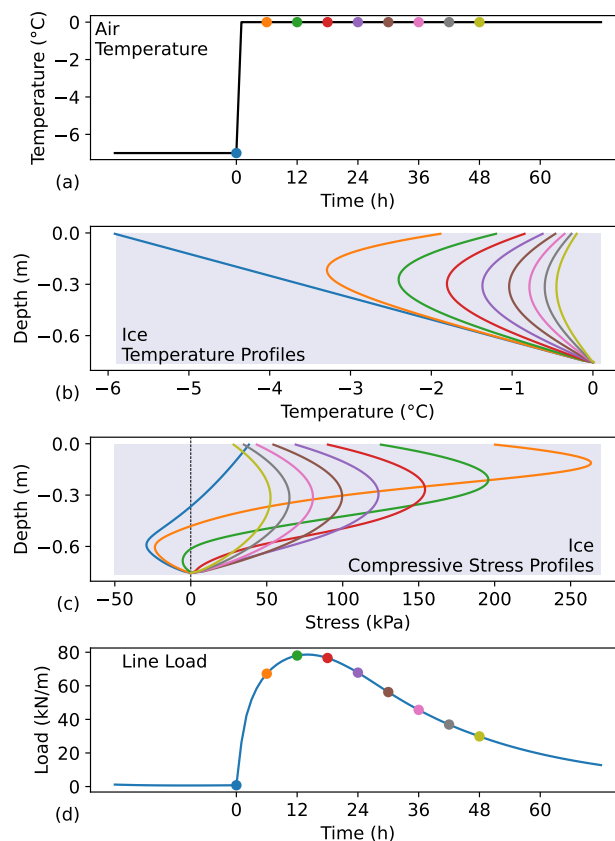


Figure 3.2: Development of a thermal load peak from (a) an air temperature step change. The dots mark reference time points. (b) Ice temperature profiles from the ice growth model shown at the the reference time points, (c) ice stress profiles derived from the ice temperature development at different depths, shown at the reference time points, and (d) line load from vertical integration of the stress profiles, with the reference time points marked.

air temperature increased to -7°C , and another month later the air temperature increased to 0°C . This last step increase is illustrated in Figure 3.2. Figure 3.2a shows the air temperature increase with time points that correspond to the other subplots. Figure 3.2b shows the ice temperature profile at these time points. After one month of growth at constant air temperature, the temperature profile is initially essentially linear with the lowest temperature at the ice–air interface. The temperature at the ice–water interface at 0.75 m depth is at 0°C . Following the air temperature increase at time point 0 (Figure 3.2a), the temperature in the ice increases fastest near the ice–air interface, leaving the lowest ice temperature in the ice center of the ice cover.

Figure 3.2c shows the depth profiles of the stress. Compressive stress is shown with a positive sign since this causes line loads, which are also positive by convention. All stress profiles are zero at the ice–water interface because the temperature is constant there and the creep rate is very high. Initially, the ice is slightly in compression at the ice–air interface, which is a residual from the temperature increase one month earlier in combination with slow creep at low temperatures. From the ice–water interface upward, the ice is in tension because the ice cover is growing, increasing in thickness and hence locally cooling. The remaining stress profile is a combination of the residual of the earlier temperature increase and the progressive cooling during ice growth. Following the air temperature change at time point 0 (Figure 3.2a), peak ice stresses are observed near the ice–air interface, which decrease in magnitude and increase in distance from ice–air interface with time. Even though initially the rate of temperature change is highest at the ice–air interface, after only 6 hours the highest stress is observed 0.1 m below the ice–air interface because the creep rates are high in the warm ice closer to the ice–air interface (not shown here, in this scenario the peak stress is in the upper 10 mm of the ice for less than 2 hours). Hence, contrary to what one might expect and consistent with measurements in the field, the vertical stress profile is never linear through ice. The vertical integration of the compressive stress results in the thermal line load shown in Figure 3.2d. The line load development shows a pronounced peak after approximately 12 hours and falls below half its peak value after 48 hours. While it is somewhat intuitive to think of the thermal load peak as the result of a significant increase in ice temperature and hence compressive stress followed by creep that reduces the stress, the complexity of the stress profile development in Figure 3.2c is indicative of our limited ability to quantitatively relate the step temperature increase in Figure 3.2a to the magnitude and shape of the thermal load peak in Figure 3.2d. The system is not linear.

3.3 Probabilistic Model

3.3.1 Snow Depth Parameterization

Modeled ice thickness was to be consistent with Equation 3.2. This was to be achieved by a suitable choice of the heat transfer coefficient from atmosphere to ice,

$$h = \min\left(h_0; \frac{k_{snow}}{H_{snow}}\right), \quad (3.3)$$

where $h_0 = 15 \text{ W}/(\text{m}^2 \text{ K})$ is the heat transfer coefficient in the absence of snow, $k_{snow} = 0.2 \text{ W}/(\text{m K})$ is the thermal conductivity of snow (e.g. Abels, 1892; Sturm et al., 1997), H_{snow} is the depth of the snow cover, and the operator $\min(a; b)$ returns the lesser of a and b . To achieve the target ice thickness, several algorithms were tried, starting with assuming that snow depth is proportional to ice thickness. That approach is attractive as it still allows for an explicit solution to the Stefan problem of ice growth (e.g. Petrich & Eicken, 2017). However, Figure 3.3 shows that assuming instantaneous snow depth at time t ,

$$H_{snow}(t) = \alpha_{si} H_{ice}(t), \quad (3.4)$$

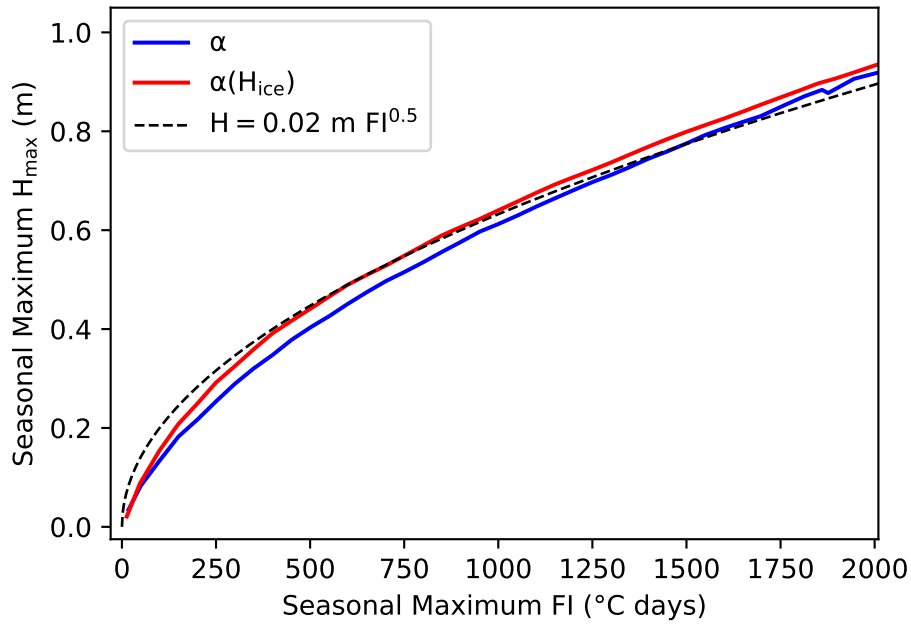


Figure 3.3: Relationship between ice thickness and freezing index for Equation 3.4 (blue line), Equation 3.5 (red line), and

where $\alpha_{si} = 0.1$ is a constant, will lead to a systematic underprediction of thickness of thin ice with respect to Equation 3.2. Instead, α_{si} was made to depend on ice thickness following

$$\alpha_{si}(t) = \begin{cases} \alpha_{si0} \frac{H_{ice}(t)}{H_{ice0}} & \text{for } 0 \leq H_{ice}(t) < H_{ice0}, \\ \alpha_{si0} & \text{else,} \end{cases} \quad (3.5)$$

where $\alpha_{si0} = 0.1$ and $H_{ice0} = 0.5$ m are constants. Hence,

$$h(t) = \begin{cases} \min \left(h_0; \frac{k_{snow} H_{ice0}}{\alpha_{si0} H_{ice}^2(t)} \right) & \text{for } 0 \leq H_{ice}(t) < H_{ice0}, \\ \min \left(h_0; \frac{k_{snow}}{\alpha_{si0} H_{ice}(t)} \right) & \text{else.} \end{cases} \quad (3.6)$$

Figure 3.3 shows that this approach yields a more conservative ice thickness estimate for thin ice and better match to Equation 3.2. However, both approaches overestimate thickness of thick ice and underestimate the thickness of thin ice with respect to the reference equation.

3.3.2 Probabilistic Model Process

The process of deriving a peak seasonal thermal line load is illustrated in Figure 3.4. Based on the air temperature record at a given location (Figure 3.4a), the water or ice in the column is either warmed or cooled at the upper surface, resulting in temperature changes at different depths (Figure 3.4b). Ice is formed where the temperature falls below the freezing point. Temperature in the ice is converted to stress in the ice at different depths (Figure 3.4c), and vertical integration of the stress results in the modeled thermal line load (Figure 3.4d). For each winter season, only the maximum line load is retained as “peak seasonal line load”.

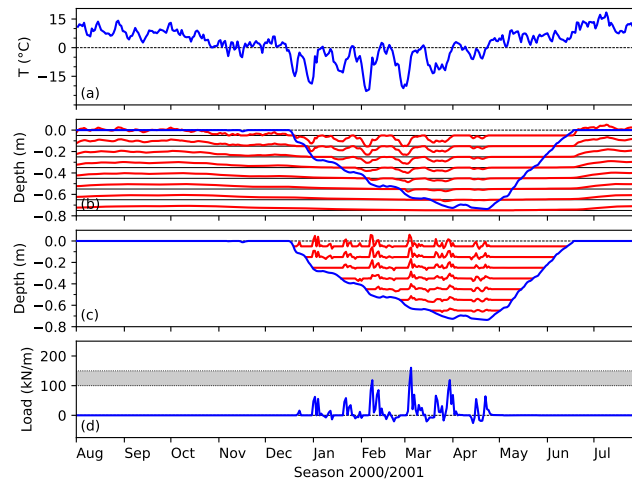


Figure 3.4: Illustration of the calculation process of thermal ice loads using a snow-free simulation. (a) Air temperature that drives the model, (b) development of calculated temperatures at different depths in the column (red spark lines) and ice thickness (blue line), (c) development of ice stress determined from ice temperatures (red spark lines) and ice thickness (blue line), (d) thermal ice load determined from ice stress.

3.3.3 Line Load Peak Distribution Function

In order to extrapolate the peak line loads with 50-year recurrence rate from a 30-year record of modeled data, the probability distribution needs to be known. This involves two aspects, one is to define the shape of the distribution, and the other to estimate of the parameters of the distribution at a given location. Figure 3.5 is used to select a distribution shape from the candidates Normal Distribution, Log-Normal Distribution, and Gumbel Distribution. Considering reservoirs one at a time, the distributions created from 31 points of modeled line loads did generally not follow an obvious distribution function. Figure 3.5 shows fits performed to three different distributions using the Probability Paper Method considering nondetects (Section 2.5). None of the distributions seems to have a clear advantage at colder locations (Figure 3.5o–ab). However, distributions differ in warmer regions. Nondetects were defined as data points with line loads < 1 kN/m. Figures 3.5a–f and i–l show distributions with nondetects. The log-normal distribution did not predict any nondetects (i.e., line load < 1 kN/m). The Gumbel distribution produced some, and the normal distribution came closest to accurately reproducing the number of years absent a significant load. Hence, the Normal Distribution cannot be excluded as an appropriate description of the modeled peak line load data and in fact may be the superior choice in warm regions.

Figure 3.6 shows an example of data plotted on Probability Paper for the Normal distribution according to Section 2.5. The data points do not deviate systematically from a straight line in this example, indicating that the Normal distribution would be a reasonable assumption. All distributions in Figure 3.5 were inspected on Probability Paper for quality control.

Other standard methods for fitting distributions performed are not shown here because the algorithms were not designed to account for nondetects. It shall be remarked here that the fitted parameters depend on the chosen fitting algorithm.

3.3.4 Design Line Load

Figure 3.7 shows a scatter plot of the design line load versus FI_{10} for 2696 locations. There is a general trend of increasing design line load with increasing FI_{10} , i.e. the line load will tend to be higher in colder regions. However, data scatter presumably due to a combination of physical effects (e.g. different weather patterns at locations of identical FI_{10}) and numerical effects (e.g. uncertainty in the distribution curve parameters due to

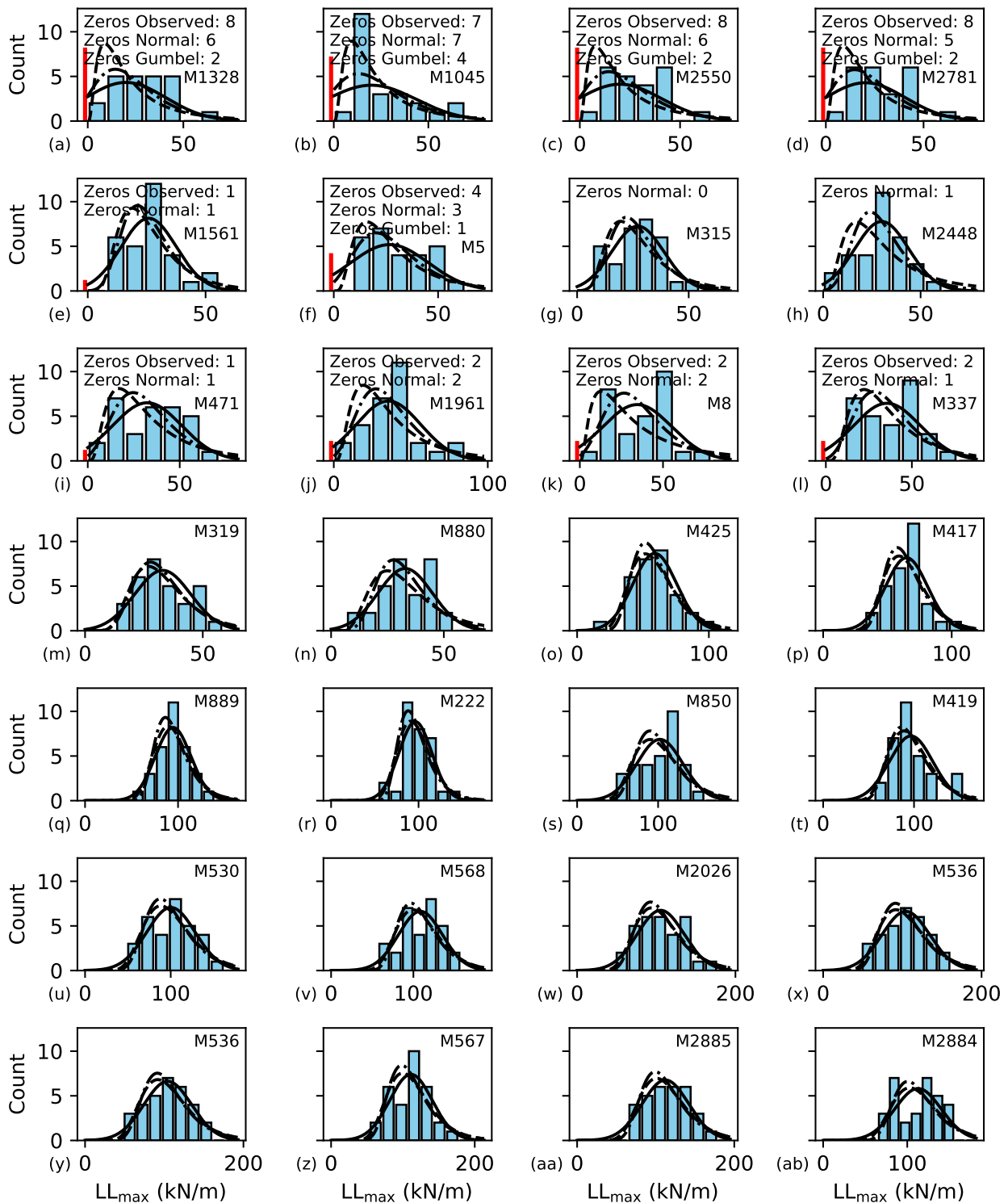


Figure 3.5: Distributions of the magnitude of 31 seasonal peak line loads at 28 reservoirs, derived from the ice load model in Sections 2.3 and 2.4 for snow-covered ice. The number of line loads ≤ 1 kN/m is indicated by the red vertical line drawn near zero. Normal (solid line), Log-Normal (dashed line), and Gumbel (dash-dotted line) distributions were fitted with the probability plot method, treating line loads ≤ 1 kN/m as nondetects (Section 2.5). Reservoir numbers are given in the plot ("M"-numbers). The expected number of winters with zero loads derived from the fitted distribution is stated in the plot if it exceeds 0.25. The reservoirs are ordered by increasing average Freezing Index. Note the different scales of the abscissae.

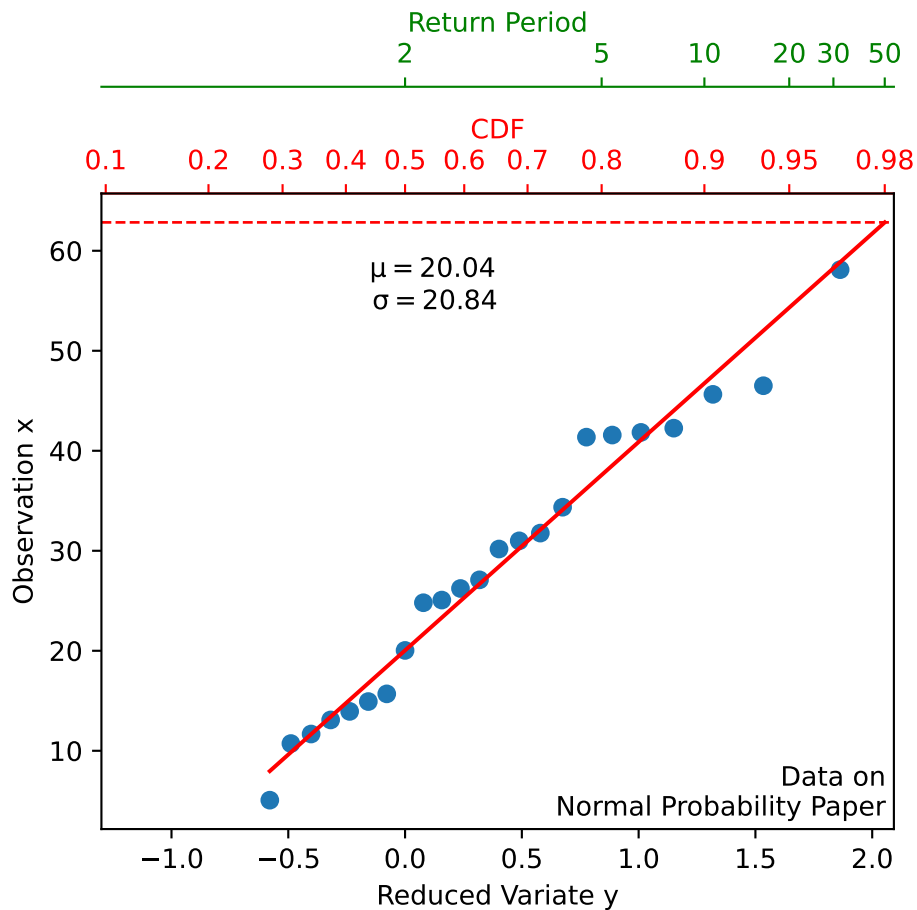


Figure 3.6: Data of reservoir M2550 in Figure 3.5c on Normal Probability Paper. The ordered observed values (“Observation x”) are shown on the ordinate while the scaled rank order number (“Reduced Variate y”) is shown on the abscissa. Eight nondetects are not shown. Fit parameters $\mu = 20.0$ kN/m and $\sigma = 20.8$ kN/m can be read off the fitted line (solid line). The value of the Cumulative Distribution Function (CDF) and associated return period is shown above the plot. In this example, the peak line load with 50-year return period is $LL_{50} = 63$ kN/m (dashed line).

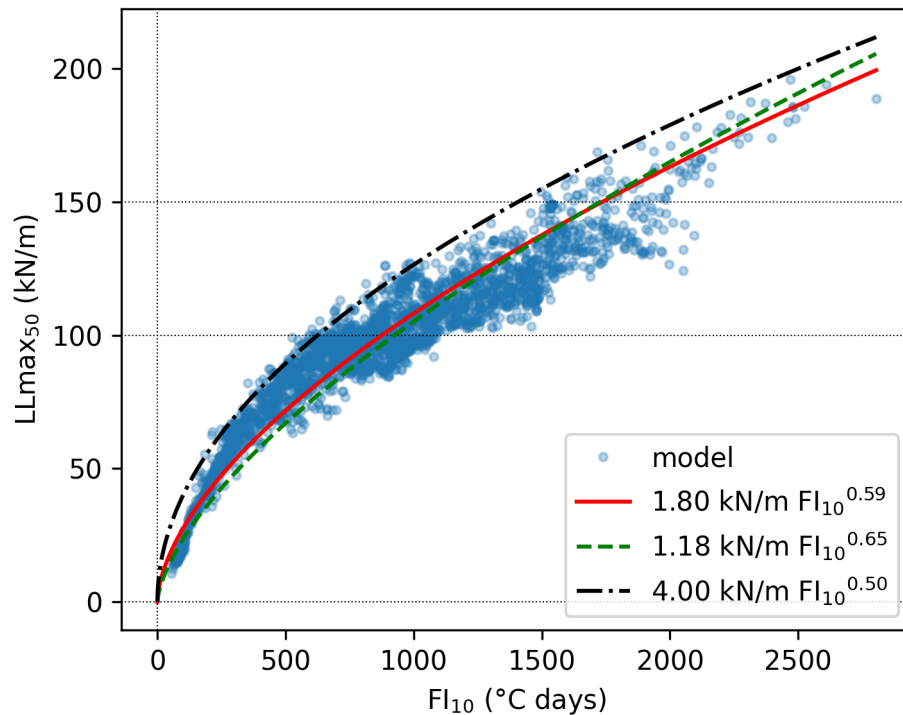


Figure 3.7: 50-year recurrence value of thermal ice load modeled for 2696 locations (dots) with FI_{10} from near 0 to 2700 °C days in Norway.

the short underlying record of 31 years). Performing a linear fit on double-logarithmic scale, the best-fit power line is

$$LL_{50} = 1.798 \text{ kN/m } FI_{10}^{0.59}, \quad (3.7)$$

where FI_{10} is in kN/m. This is almost identical to the result from the deterministic model (Equation 3.12, Figure 3.7), and similar to the result from explicit equation. While data points fall into a band of $\pm 20\%$ of the best-fit line, the actual scatter of the data is considerably narrower for FI_{10} above 1000 to 2000 °C days. An upper bound of the scattered data is approximated by

$$LL_{50} = 4 \text{ kN/m } FI_{10}^{0.5}. \quad (3.8)$$

3.3.5 Ice Stress at Peak Load

Figure 3.8 shows the average ice stress at the time of peak line load determined from the probabilistic model. While the average, not including the zeros, is 143 kPa, one notices significant differences between the reservoirs and years. Inter-annual differences may be due to differences in temperature and ice thickness.

3.4 Deterministic Model

3.4.1 Model Input

Based on seNorge weather data at 144 locations in Norway, 10-year minimum daily air temperature (Figure 3.9) and 10-year maximum daily temperature rise (Figure 3.10) were plotted against the 10-year Freezing Index,

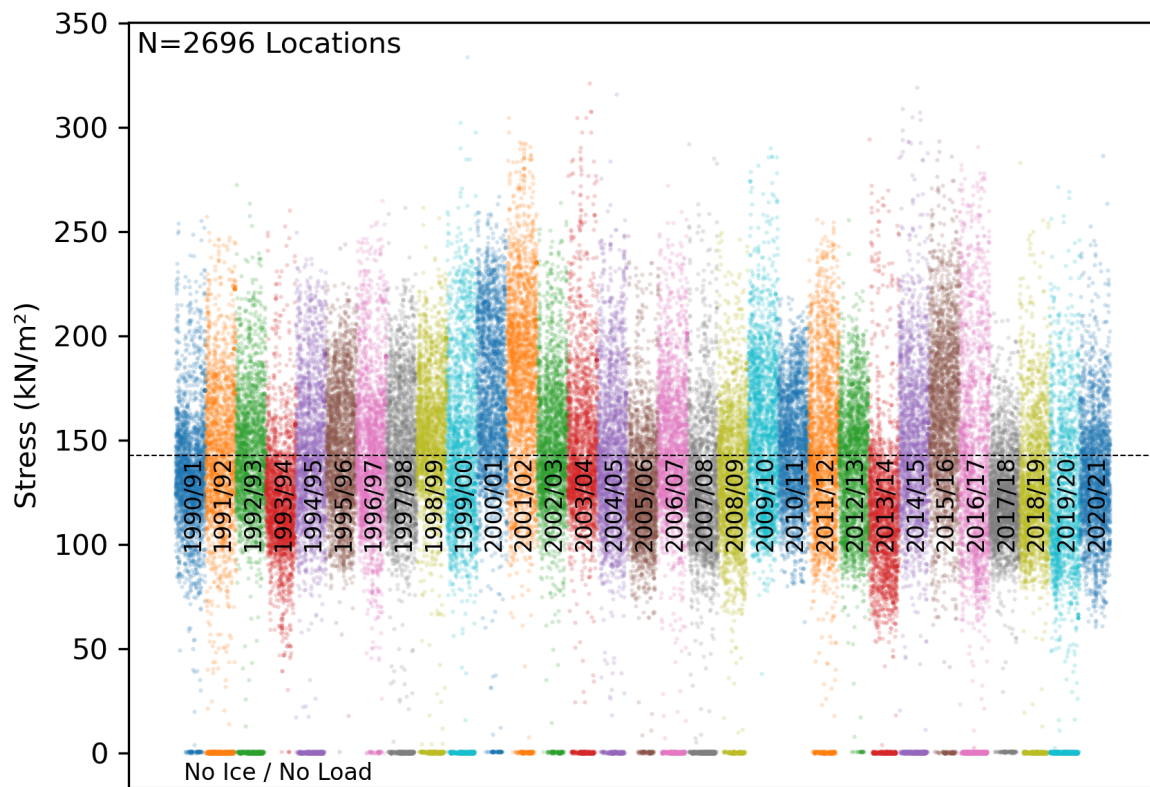


Figure 3.8: Scatter plot of average ice stress at peak line load, i.e. line load divided by ice thickness at the time, for 2696 reservoirs over 31 winters. Dots at zero indicate absence of either ice or ice load. The horizontal line indicates the average. Each dot represents one data point, colors are used to visually separate the seasons.

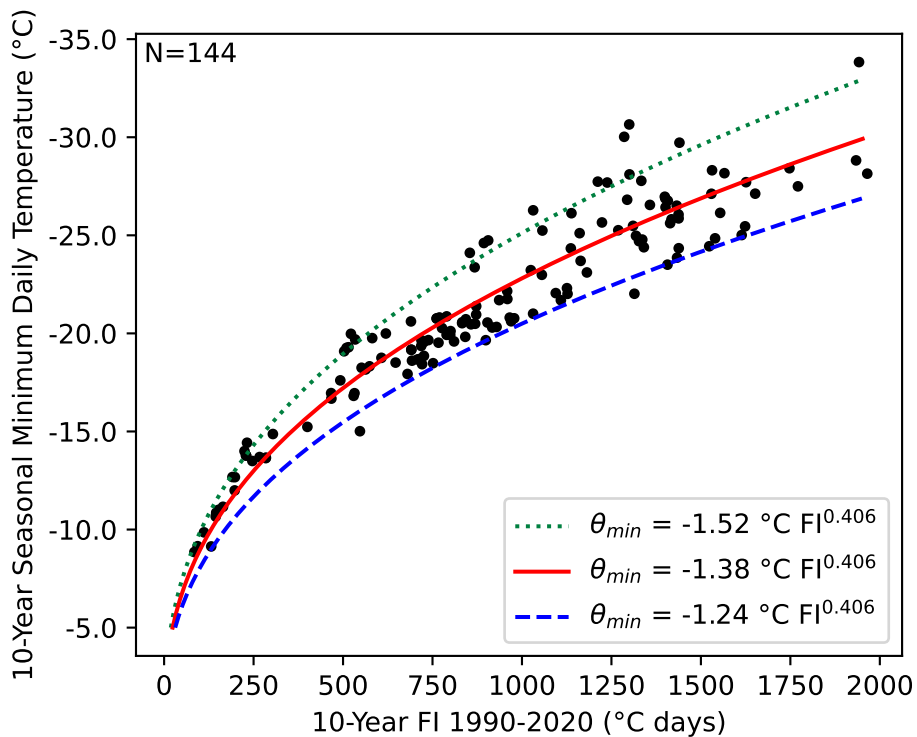


Figure 3.9: Expected 10-year minimum daily air temperature as a function of 10-year Freezing Index (FI_{10}) based on 144 locations from seNorge data. The best fit line is solid red, while dashed and dotted lines outline lower and upper limits used Table 2.2.

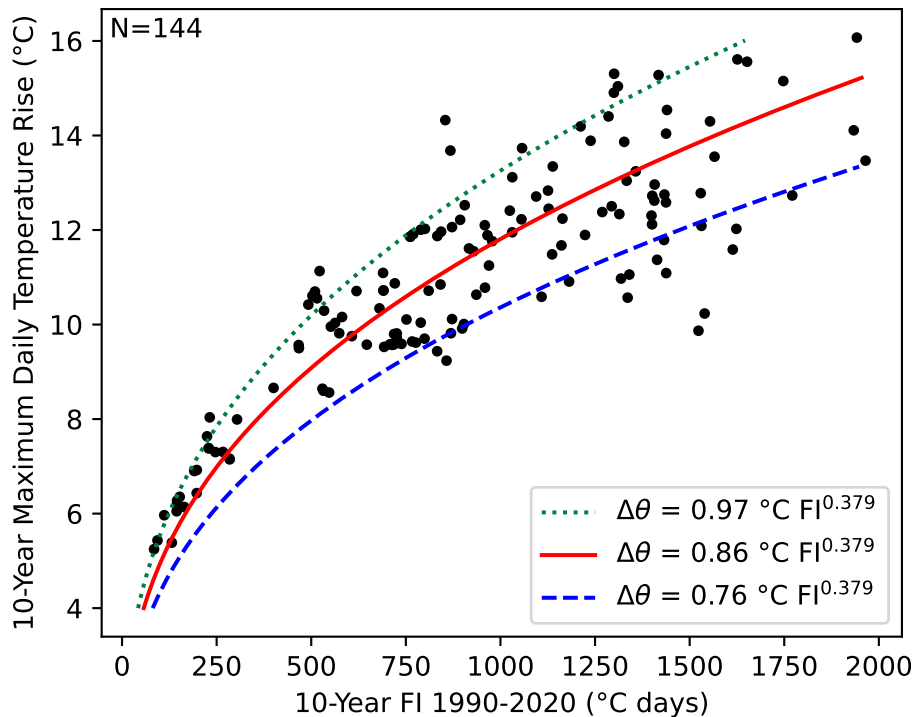


Figure 3.10: Expected 10-year maximum daily air temperature rise as a function of 10-year Freezing Index (FI_{10}) based on 144 locations from seNorge data. The best fit line is solid red, while dashed and dotted lines outline lower and upper limits used Table 2.2

FI_{10} . The best-fit lines are

$$\theta_{min,10} = -1.38 \text{ } ^\circ\text{C } FI_{10}^{0.406}, \quad \text{and} \quad (3.9)$$

$$\Delta\theta_{10} = 0.86 \text{ } ^\circ\text{C } FI_{10}^{0.379}. \quad (3.10)$$

3.4.2 Design Line Load

The relationship between thermal line loads and 10-year freezing index based on parameters in Table 2.2 is illustrated in Figure 3.11. Besides the nominal (“Reference”) parameter set, parameter sets that result in lower (“Low”) and higher (“High”) line loads are given, with coefficients changed by approximately 10%. Thermal line loads are higher in the snow-free scenario (Scenario I) than in the lightly snow-covered scenario (Scenario II). They are expected to increase with freezing index, and the Reference line can be approximated by

$$LL = 1.56 \text{ kN/m } FI_{10}^{0.72} \quad \text{for the snow-free scenario, and} \quad (3.11)$$

$$LL = 1.18 \text{ kN/m } FI_{10}^{0.65} \quad \text{for the snow-covered scenario,} \quad (3.12)$$

where the 10-year Freezing Index FI_{10} is in multiples of $^\circ\text{C days}$. Line loads in the lightly snow-covered scenario barely exceed 150 kN/m. Equation 3.12 is also plotted in Figure 3.7 where it coincides with the best-fit line of the probabilistic model.

3.5 Explicit Equation

3.5.1 Design Line Load

The sensitivity to FI_{10} of the term in brackets in Equation 2.30 shall be investigated. Using the relationships from Table 2.2, we denote the parameters c_1 and c_2 for

- ice thickness: c_1^H and c_2^H ,
- minimum temperature c_1^0 and c_2^0 , and
- temperature rise c_1^Δ and c_2^Δ .

Starting with the expression hH_{ice} in Equation 2.30 and the definition of h for the snow-covered case (Table 2.2),

$$hH_{ice} = \frac{H_{ice}}{\frac{1}{c_1^H} + c_2^H H_{ice}}, \quad (3.13)$$

$$= \frac{c_1^H H_{ice}}{1 + c_1^H c_2^H H_{ice}}, \quad (3.14)$$

and hence

$$1 + \frac{k_i}{hH_{ice}} = 1 + k_i \left(c_2^H + \frac{1}{c_1^H H_{ice}} \right) \quad (3.15)$$

we see that Equation 3.15 is rather insensitive to H_{ice} for all but the thinnest ice. For example, between $H_{ice} = 0.2 \text{ m}$ and 1.5 m , this expression changes only from 2.6 to 2.1. We therefore introduce constant C and substitute by setting

$$C = 1 + \frac{k_i}{hH_{ice}}, \quad (3.16)$$

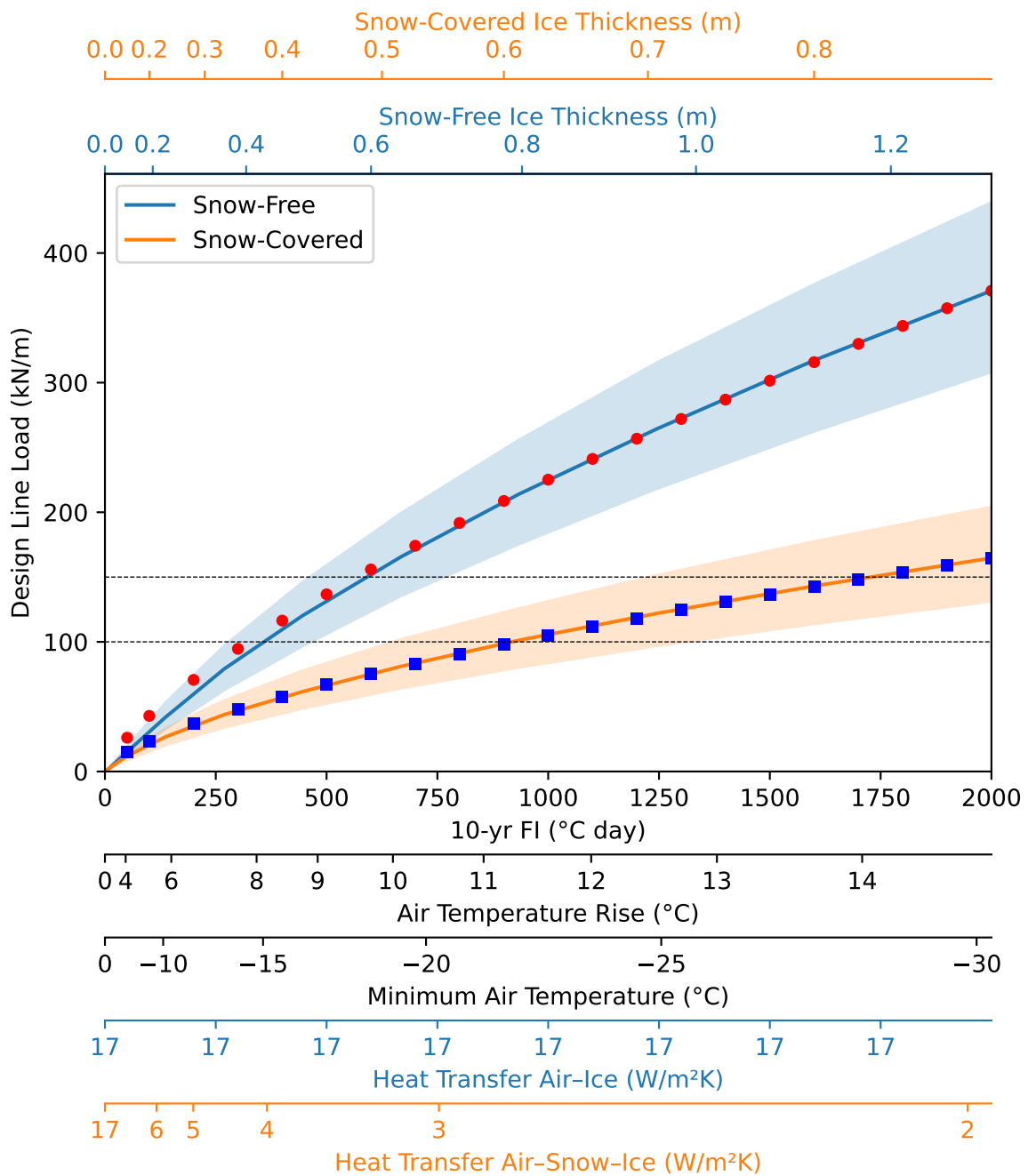


Figure 3.11: Design line load from the deterministic model for the parameters given in Table 2.2. Red dots and blue squares follow the equations given for the snow-free and snow-covered scenarios, respectively. The shaded areas indicate the range between low and high scenarios. Ice thickness, air temperature rise, and minimum air temperature are inputs directly calculated from FI_{10} . The heat transfer coefficient is given for ice of indicated thickness.



with $C \approx 2.2$.

The sum

$$1 + \alpha_d \frac{\Delta\theta}{\theta_0} = 1 + \alpha_d \frac{c_1^\Delta}{c_1^0} FI^{c_2^\Delta - c_2^0} \quad (3.17)$$

is approximately constant since the difference $c_2^\Delta - c_2^0 \approx -0.05$. I.e., this becomes

$$D = 1 + \alpha_d \frac{\Delta\theta}{\theta_0}, \quad (3.18)$$

$$(3.19)$$

where $D \approx 0.48$. Hence, from Equation 2.22,

$$LL = H_{ice} \sigma_0 \left[\frac{A}{B} \frac{2k_i}{\rho_i c_i} \frac{\Delta\theta}{C} \frac{1}{H_{ice}^2} \left(\frac{D\theta_0}{2CT_1} \right)^m \right]^{\frac{1}{n}}. \quad (3.20)$$

If we express $\Delta\theta$, θ_0 , and H_{ice} in the square brackets in terms of FI we get

$$LL = H_{ice} \sigma_0 \left[\frac{A}{B} \frac{2k_i}{\rho_i c_i} \frac{c_1^\Delta}{C} \frac{1}{(c_1^H)^2} \left(\frac{Dc_1^0}{2CT_1} \right)^m \right]^{\frac{1}{n}} FI^{\frac{c_2^\Delta - 2c_2^H + mc_2^0}{n}} \quad (3.21)$$

Due to all factors c_2 of the same order of magnitude and a relatively large factor n in the denominator, the dependence of σ_r on FI (i.e. $\propto FI^{0.034} \approx 1.25$) is much less than the dependence of H_{ice} on FI (i.e. $\propto FI^{0.5}$). Hence, as a first-order estimate one would expect that the thermal line load is proportional to ice thickness multiplied by a representative stress σ_r that is rather independent of the FI_{10} of a given location. Substituting all constants, we get

$$\sigma_r = 100 \text{ kPa} \times \left[\frac{2 \times 10^5}{3.96} \frac{2 \times 2}{920 \times 2100} \frac{1.05}{2.2} \frac{1}{0.02 \times 0.02} \left(\frac{0.48 \times 1.38}{2 \times 2.2} \right)^{1.92} \right]^{1/3.7} \times 1.25 \quad (3.22)$$

$$= 172 \text{ kPa}. \quad (3.23)$$

Hence, at a given location in Norway assuming a light snow cover, the deterministic estimate of peak seasonal line load based on peak seasonal ice thickness is

$$LL = 170 \text{ kPa } H_{ice}. \quad (3.24)$$

For snow-free ice, we have $c_1^H = 0.01$ instead of 0.02, hence $C = 1.2$ instead of $C = 2.2$, and a value of FI raised to its exponent of 0.75 instead of 1.25. Hence, $\sigma_r \approx 242 \text{ kPa}$.

The key result is that the representative ice stress at peak load, σ_r , is a constant for prescribed snow conditions, and hence the peak thermal ice load is proportional to ice thickness (Equation 2.22).

Chapter 4

Discussion

4.1 Explicit Equation

Rudimentary efforts have been performed to evaluate the quality of the explicit equation. While the method is able to reproduce the presented Reference results of the Deterministic Model (typical error of $< 10\%$ or 3 kN/m , whichever is greater), the bounds of validity of this method are currently not well established. However, known shortcomings include that the method will

- vastly overestimate the load if the starting temperature is low and the step change is small (e.g. an air temperature increase from -30 to -28 °C. In this case, the method assumes the signal persists for too long.),
- underestimate the load if the starting temperature is low and the step change reaches temperatures close to the melting point (the representative temperature of the temperature of the ice is overestimated in this case, exaggerating creep),
- slightly overestimates loads (20% or 10 kN/m) in the presence of substantial thermal surface insulation ($\leq 1 \text{ W}/(\text{m}^2 \text{ K})$).

While this model is physically based, it is tuned to the Reference case of the Deterministic Model. It should not be expected to produce reasonable results for other parameters, especially not for different coefficients of the stress model (A , B , n , m).

The Explicit Equation assumes that thermal loads are brought about by well-defined temperature conditions and from that, predicts that a representative stress exists during a load peak. The well-defined conditions stem from the expressions Equation 3.9 and 3.10 that were fitted to scattered air temperature data. Hence, while there may be such a thing as a representative stress corresponding to a representative load peak, not every seasonally maximum peak is a representative peak. This is illustrated by the scatter in Figure 3.8 that shows that the average ice stress during the seasonal peak event is expected to spread broadly. However, the average ice stress during the extrapolated 50-year line load event seems to be well-defined, as can be seen by the square-root bound in Figure 3.7.

4.2 Peak Ice Load Probability Distribution

Maybe surprisingly, the seasonal peak line loads did not follow the GEV distribution. The GEV distribution applies only if both the parent distribution of annual peaks and the number of annual maxima is sufficiently large. The meaning of sufficiently large depends on the (usually unknown) underlying distribution. With a handful of candidate peaks each winter and 31 years of data, the data basis for an individual reservoir is likely too small to assume asymptotic convergence. This means that the 31 years of data will be sampled from an



unknown distribution. In addition, the distribution of annual maxima is not stationary as ice thickness increases during the season and with it the likelihood of seeing a high load event.

Apart from investigating the histograms, the obtained distributions were also plotted on probability paper to identify the most suitable probability distribution function. Given the small data set at each location and differences between locations, the analysis was anecdotal. However, there was no indication that any of the tested distribution consistently outperformed the Normal distribution.

4.3 Other Effects

Several effects have not been considered in this study. Thin ice could possibly buckle before exerting the full theoretical load onto the dam (Michel, 1970), the elastic modulus of ice depends on inclusions and crystal structure (Kharik et al., 2018), a thick snow cover could nearly insulate the ice or even depress it below the water, and solar radiation can induce an ice temperature signal. The shape and stiffness of dams was not considered, nor was the difference between local and global line loads addressed. Buckling could be addressed through an equation that describes the upper possible limit of loads. In the absence of these considerations, the predicted loads may be too high. However, modeling ice properties and heavy snow loads would require a dedicated study. Absorption of solar radiation could be introduced into the model but would require a handle on typical atmospheric and optical properties of the snow cover. Significant solar irradiation is typically absent in parts of Norway at the height of winter. However, in its presence a diurnal signal could introduce thermal loads while general warming of the ice would reduce loads due to increased creep.

Chapter 5

Conclusion

This study investigated a method to introduce a thermal ice load that takes account for the regional differences in mainland Norwegian climate. While the project started with a focus on regions with low freezing degree days, the project reference group expressed the desire to extend the scope across the entire spectrum of Norwegian environmental conditions. During preliminary investigations into this matter, it became clear that attention ought to be paid to the regional differences in snow cover throughout Norway, an aspect that should be taken up in future studies. Instead, this project assumed “lightly snow-covered ice” throughout, consistent with the ice thickness equation currently found in the regulations (NVE, 2003). Also, inhomogeneous or differing ice properties were not considered explicitly. In order to be relevant to coastal regions in Norway with occasional melting temperatures in winter, ice conditions were expressed in terms of the Freezing Index rather than Freezing Degree Days. This distinction is immaterial for regions that are consistently cold throughout winter.

Ice loads were calculated with a probabilistic model, deterministic model, and an explicit equation. The results of the methods were consistent, albeit a bit uncertain. A methodological part of the problem is that line load probability distributions were derived for reservoirs individually, based on data of only 31 years. Given considerable inter-annual variability, there was uncertainty in the parameters derived of the distribution, leading to scattered results. An upper bound for the design line load was

$$LL_{50} = 4 \text{ kN/m } FI_{10}^{0.5}, \quad (5.1)$$

while the best fit line is up to 20 kN/m lower.

In order to evaluate line loads probabilistically, a method from the biomedical field was introduced to the field of ice load modeling. Especially in Norwegian coastal regions, the peak ice loads may be zero in some winters. The years of absent line loads were treated like nondetects in other fields, i.e. data points that are there but lie below the limit at which they can be quantified. It turned out that the Normal distribution described the histogram of line loads at any given reservoir at least as well as other distributions tested, while also giving superior predictions of the frequency of ice load-free years.

A deterministic ice load model was developed based on a-priori relationships between the local Freezing Index and ice thickness, minimum air temperature, and maximum daily air temperature rise. If these relationships differ across the globe then the results of this study may not be universally applicable either. The relationships were determined for Norway between the local Freezing Index and either minimum air temperature or maximum daily air temperature rise. The best fit line removed the scatter of the data, resulting in model results that were free from scatter. A subsequent sensitivity analysis helped identify the parameters the models are most sensitive to, ice thickness and ice temperature being among the most important.

The deterministic model was reduced to an explicit equation. This equation expressed the design line load as the product of ice thickness and a characteristic ice stress. It also suggested that the interdependencies of ice thickness, minimum air temperature and air temperature rise are such that the characteristic stress is almost independent of the reservoir: under the current climatic conditions in Norway, and assuming “lightly



snow-covered ice” everywhere. Hence, Equation 5.1 is an engineering equation that may be interpreted as the product of ice thickness with a constant characteristic ice stress.



Bibliography

- Abels, H. F. (1892). Beobachtungen der täglichen Periode der Temperatur im Schnee und Bestimmung des Wärmeleistungsvermögens des Schnees als Function seiner Dichtigkeit. *Repertorium für Meteorologie*, 16, 1–53.
- Adolfi, E., & Eriksson, J. (2013). *Islastens inverkan på brottsannolikheten för glidning och stjälpning av betongdammar*.
- Anscombe, F. J. (1973). Graphs in Statistical Analysis. *The American Statistician*, 27(1), 17–21. <https://doi.org/10.2307/2682899>
- Azarnejad, A., & Hrudehy, T. M. (1998). A numerical study of thermal ice loads on structures. *Canadian Journal of Civil Engineering*, 25(3), 557–568. <https://doi.org/10.1139/I97-119>
- Bergdahl, L. (1978). *Thermal ice pressure in lake ice covers* [Doctoral dissertation, Chalmers tekniska högskola].
- Brent, A. D., Voller, V. R., & Reid, K. J. (1988). Enthalpy-Porosity Technique for Modeling Convection-Diffusion Phase Change: Application to the Melting of a Pure Metal. *Numerical Heat Transfer*, 13(3), 297–318. <https://doi.org/10.1080/10407788808913615>
- Carter, D., Sodhi, D., Stander, E., Caron, O., & Quach, T. (1998). Ice Thrust in Reservoirs. *Journal of Cold Regions Engineering*, 12(4), 169–183. [https://doi.org/10.1061/\(ASCE\)0887-381X\(1998\)12:4\(169\)](https://doi.org/10.1061/(ASCE)0887-381X(1998)12:4(169))
- Coles, S. (2001). *An Introduction to Statistical Modeling of Extreme Values*. Springer London. <https://doi.org/10.1007/978-1-4471-3675-0>
- Comfort, G., Gong, Y., Singh, S., & Abdelnour, R. (2003). Static ice loads on dams. *Canadian Journal of Civil Engineering*, 30(1), 42–68. <https://doi.org/10.1139/I02-080>
- Côté, A., Taras, A., Comfort, G., & Morse, B. (2016). Static Ice Loads at Dam Face and at Far Field. *Proceedings of the 23rd IAHR International Symposium on Ice, Ann Arbor, Michigan, USA*, 8pp.
- Cox, G. F. N. (1984). A preliminary investigation of thermal ice pressures. *Cold Regions Science and Technology*, 9(3), 221–229. [https://doi.org/10.1016/0165-232X\(84\)90069-7](https://doi.org/10.1016/0165-232X(84)90069-7)
- Drouin, M. (1976). *Forces d'impact et d'expansion thermique de la glace sur les ouvrages du Complexe La Grande*. Direction Ingénierie, Société d'énergie de la Baie James. Montreal, Canada.
- Fisher, R. A., & Tippett, L. H. C. (1928). Limiting forms of the frequency distribution of the largest or smallest member of a sample. *Mathematical Proceedings of the Cambridge Philosophical Society*, 24(2), 180–190. <https://doi.org/10.1017/S0305004100015681>
- Foss, A. B. (2017). *Islast mot dammer med varierende vannstand* [Master's thesis, NTNU].
- Fransson, L. (1988). *Thermal ice pressure on structures in ice covers* [Doctoral dissertation, Luleå University of Technology].
- Gebre, S., Alfredsen, K., Lia, L., Stickler, M., & Tesaker, E. (2013). Review of Ice Effects on Hydropower Systems. *Journal of Cold Regions Engineering*, 27(4), 196–222. [https://doi.org/10.1061/\(ASCE\)CR.1943-5495.0000059](https://doi.org/10.1061/(ASCE)CR.1943-5495.0000059)
- Gumbel, E. J. (1954). *Statistical Theory of Extreme Values and Some Practical Applications. A Series of Lectures*. (PB175818). National Bureau of Standards, Washington, D. C. Applied Mathematics Div.
- Gumbel, E. J. (1958). *Statistics of extremes*. Columbia University Press.



- Hellgren, R., Petrich, C., Arntsen, B., & Malm, R. (2022). Ice load measurements on Råtán concrete dam using different sensor types. *Cold Regions Science and Technology*, 193, 103425. <https://doi.org/10.1016/j.coldregions.2021.103425>
- Helsel, D. (2010). Much ado about next to nothing: Incorporating nondetects in science. *The Annals of Occupational Hygiene*, 54(3), 257–262. <https://doi.org/10.1093/annhyg/mep092>
- Hosking, J. R. M. (1990). L-Moments: Analysis and Estimation of Distributions Using Linear Combinations of Order Statistics. *Journal of the Royal Statistical Society: Series B (Methodological)*, 52(1), 105–124. <https://doi.org/10.1111/j.2517-6161.1990.tb01775.x>
- Hosking, J. R. M., Wallis, J. R., & Wood, E. F. (1985). Estimation of the Generalized Extreme-Value Distribution by the Method of Probability-Weighted Moments. *Technometrics*, 27(3), 251–261. <https://doi.org/10.1080/00401706.1985.10488049>
- Hovde, E., Engseth, M., Konow, T., & Kristiansen, A. (2018). Probabilistic Analysis of a Gravity Dam in Norway. *Proceedings of the Twenty-Sixth International Congress on Large Dams (ICOLD)*, 10.
- ISO13793. (2001). *Thermal performance of buildings - Thermal design of foundations to avoid frost heave (ISO13793:2001)*. International Organization for Standardization. Geneva, Switzerland.
- Jenkinson, A. F. (1955). The frequency distribution of the annual maximum (or minimum) values of meteorological elements. *Quarterly Journal of the Royal Meteorological Society*, 81(348), 158–171. <https://doi.org/10.1002/qj.49708134804>
- Kharik, E., Morse, B., Roubtsova, V., Fafard, M., Côté, A., & Comfort, G. (2018). Numerical studies for a better understanding of static ice loads on dams. *Canadian Journal of Civil Engineering*, 45(1), 18–29. <https://doi.org/10.1139/cjce-2017-0142>
- Kvande, T., Tajet, H. T. T., & Hygden, H. O. (2023). *Klimadata for termisk dimensjonering og frostsikring (Byggedetaljer 451.021)*. SINTEF Community.
- Lia, L., Folden, B. O., Finanger, H., Tesaker, E., Hoseth, K. A., & Fransson, L. (2002). *Islast mot dammer (No. 82-2002)*. EBL Kompetanse AS.
- Lussana, C., Tveito, O. E., & Uboldi, F. (2016). *seNorge v2.0, Temperature (METreport No. 14/2016)*. Norwegian Meteorological Institute.
- Makkonen, L. (2006). Plotting Positions in Extreme Value Analysis. *Journal of Applied Meteorology and Climatology*, 45(2), 334–340. <https://doi.org/10.1175/JAM2349.1>
- Makkonen, L. (2008). Problems in the extreme value analysis. *Structural Safety*, 30(5), 405–419. <https://doi.org/10.1016/j.strusafe.2006.12.001>
- Makkonen, L., & Tikanmäki, M. (2019). An improved method of extreme value analysis. *Journal of Hydrology X*, 2, 100012. <https://doi.org/10.1016/j.hydroa.2018.100012>
- Michel, B. (1970). *Ice Pressure on Engineering Structures (Cold Regions Science and Engineering Monograph No. III-B1b)*. Cold Regions Research and Engineering Laboratory. Hanover, New Hampshire.
- Michel, B. (1971). *Winter Regime of Rivers and Lakes (Cold regions science and engineering monograph No. III-B1A)*. U.S. Army Cold Regions Research and Engineering Laboratory.
- Morse, B., Stander, E., Côté, A., Morse, J., Beaulieu, P., Tarras, A., Noël, P., & Pratt, Y. (2009). Ice Interactions at a Dam Face. In *Proceedings of the 15th Workshop on River Ice, St. John's, Newfoundland and Labrador, Canada, 15–17 June 2009* (pp. 353–363).
- Morse, B., Stander, E., Côté, A., Richard, M., & Desmet, V. (2011). Stress and Strain Dynamics in a Hydro-Electric Reservoir Ice Sheet. In *Proceedings of the 16th Workshop on the Hydraulics of Ice Covered Rivers, Winnipeg, MB, Canada, 18–22 September 2011* (pp. 303–316).
- Mydland, J. O., & Eklund, H. (2021). *Probabilistiske analyser av betongdammer - Fase 3*. Energi Norge AS.
- NVE. (2003). *Retningslinje for laster og dimensjonering (Retningslinje)*. Norges vassdrags- og energidirektorat.
- Palmer, A., & Croasdale, K. (2012). *Arctic offshore engineering*. World Scientific. <https://doi.org/10.1142/8283>
- Papalexioiu, S. M., & Koutsoyiannis, D. (2013). Battle of extreme value distributions: A global survey on extreme daily rainfall. *Water Resources Research*, 49(1), 187–201. <https://doi.org/10.1029/2012WR012557>
- Patankar, S. (1980). *Numerical Heat Transfer and Fluid Flow*. CRC Press. <https://doi.org/10.1201/9781482234213>



- Pearson, K. (1936). Method of Moments and Method of Maximum Likelihood. *Biometrika*, 28(1/2), 34–59. <https://doi.org/10.2307/2334123>
- Petrich, C., & Eicken, H. (2017). Overview of sea ice growth and properties. In D. N. Thomas (Ed.), *Sea Ice* (1st ed., pp. 1–41). Wiley. <https://doi.org/10.1002/9781118778371.ch1>
- Petrich, C., Langhorne, P. J., & Sun, Z. F. (2006). Modelling the interrelationships between permeability, effective porosity and total porosity in sea ice. *Cold Regions Science and Technology*, 44(2), 131–144. <https://doi.org/10.1016/j.coldregions.2005.10.001>
- Petrich, C., Sæther, I., Fransson, L., Sand, B., & Arntsen, B. (2015). Time-dependent spatial distribution of thermal stresses in the ice cover of a small reservoir. *Cold Regions Science and Technology*, 120, 35–44. <https://doi.org/10.1016/j.coldregions.2015.09.003>
- Petrich, C., Sæther, I. V., O'Sadnick, M., & Arntsen, B. (2020). Static ice loads on a dam in a small Norwegian reservoir. In *Proceedings of the 25th IAHR International Symposium on Ice* (8pp).
- Petrich, C., & Arntsen, B. (2018). An overview of trends and regional distribution of thermal ice loads on dams in Norway. *Proceedings of the 26th International Congress of the International Commission of Large Dams (ICOLD), Vienna, Austria, 1-7 July 2018, Q.101, R.72*, 1210–1224.
- Qiu, W., Li, K., Zhao, X., Hou, Z., Wang, Z., & Yu, J. (2024). Prototype observation and analysis of static ice pressure on reservoir piers in cold regions. *Cold Regions Science and Technology*. <https://doi.org/10.1016/j.coldregions.2024.104352>
- Sæther, I. V. (2019). *Methods for prediction of thermally-induced ice loads on dams and hydro-electrical structures* (No. 2019/19). Norut Narvik.
- Sandaker, T. K. (2018). *Hensfoss - Probabilistiske beregninger av lamelldam*. Norkonsult.
- Santner, J. F. (1973). *An Introduction to Gumbel, Or Extreme-value Probability Paper*. Training Manual. U.S. Environmental Protection Agency.
- Shumway, R. H., Azari, R. S., & Kayhanian, M. (2002). Statistical approaches to estimating mean water quality concentrations with detection limits. *Environmental Science & Technology*, 36(15), 3345–3353. <https://doi.org/10.1021/es0111129>
- Sinha, N. K. (1983). Creep model of ice for monotonically increasing stress. *Cold Regions Science and Technology*, 8(1), 25–33. [https://doi.org/10.1016/0165-232X\(83\)90014-9](https://doi.org/10.1016/0165-232X(83)90014-9)
- Straub, A. L., & Wegmann, F. J. (1965). Determination of Freezing Index Values. *Highway Research Record*, (68), 17–30.
- Sturm, M., Holmgren, J., König, M., & Morris, K. (1997). The thermal conductivity of seasonal snow. *Journal of Glaciology*, 43(143), 26–41. <https://doi.org/10.3189/S0022143000002781>
- Tajet, H. T. T., & Grinde, L. (2022). *Snølaster i Norge 1961-2020* (Rapport No. 36-2022). SINTEF Community.
- Taras, A., Côté, A., Comfort, G., Thériault, L., & Morse, B. (2011). Measurements of ice thrust at Arnprior and Barrett Chute dams. In *Proceedings of the 16th Workshop on the Hydraulics of Ice Covered Rivers, Winnipeg, MB, Canada* (pp. 317–328).
- Virtanen, P., Gommers, R., Oliphant, T. E., Haberland, M., Reddy, T., Cournapeau, D., Burovski, E., Peterson, P., Weckesser, W., Bright, J., van der Walt, S. J., Brett, M., Wilson, J., Millman, K. J., Mayorov, N., Nelson, A. R. J., Jones, E., Kern, R., Larson, E., ... van Mulbregt, P. (2020). SciPy 1.0: Fundamental algorithms for scientific computing in Python. *Nature Methods*, 17(3), 261–272. <https://doi.org/10.1038/s41592-019-0686-2>
- Wilde, M. W., & Johansson, F. (2016). *Probabilistic Model Code for Concrete Dams* (No. 292). Energiforsk.
- Xie, Y. (1992). Laws of ice sheet generation and disappearance in Shengli Reservoir, Heilongjiang. *Journal of Glaciology and Geocryology*, 14(2), 168–173.



SINTEF

Technology for a better society